Volume 1, Issue 1 — July — December-2015

E C O R F A N

Journal-Democratic Republic of Congo

ISSN-On line: 2414-4924

ECORFAN®

Indexing

Academic Google

ECORFAN-Democratic Republic of Congo

ECORFAN Journal-Democratic Republic of Congo, Volume 1, Issue 1, July-December 2015, is a journal edited semestral by ECORFAN. 6593 Kinshasa 31Rép. DémocratiqueduCongo.WEB:www.ecorfan.org/DemocraticRepublicofCongo/,journal@ecorfan.org. Editor in Chief: RAMOS-ESCAMILLA, María. ISSN-On line: 2414-4924. Responsible for the latest update of this number ECORFAN Computer Unit. ESCAMILLA-BOUCHÁN, Imelda, LUNA-SOTO, Vladimir, 6593 Kinshasa 31Rép. Démocratique du Congo, last updated December 31, 2015.

Editorial Board

Arbitration Committee

Presentation

ECORFAN Journal-Democratic Republic of Congo is a research journal that publishes articles in the areas of:

Image and Signal Processing, Control, Digital System, Optimization, Artificial Intelligence, Fuzzy Logic, Mathematical Modelling, Computational Mathematics and Computer Science

In Pro-Research, Teaching and Training of human resources committed to Science. The content of the articles and reviews that appear in each issue are those of the authors and does not necessarily the opinion of the editor in chief.

In Number 1st presented an article Brain Tumor and Vascular Structures Segmentation Applied in Computer Assisted Surgery *by ILUNGA-MBUYAMBA, Elisee and AVIÑA-CERVANTES, J. G. with adscription in the Universidad de Guanajuato, in the next Section an article* Kalman filter for skin-colored object tracking *by H.-AGUIRRE-RAMOS, J. G., AVINA-CERVANTES, E. and ILUNGA, Mbuyamba with adscription in the Universidad de Guanajuato, in the next Section an article:* Bayesian classification of oranges using image processing *by ILUNGA-MBUYAMBA, Elisée and AVIÑA-CERVANTES, Juan GABRIEL with adscription in the U Universidad de Guanajuato, in the next Section an article* Segmentation of vascular structures around brain tumors using region growing on Frangi vesselness *by* ILUNGA-MBUYAMBA, Elisee, AVIÑA-CERVANTES, Juan Gabriel and AGUIRRE-RAMOS, Hugo *with adscription in the Universidad de Guanajuato, in the next Section an article:* Multiumbral optimal segmentation through a metaheuristic optimization algorithm *by MONTOYA-AGUILAR, Merary, CRUZ-DUARTE, Jorge Mario and AVIÑA-CERVANTES, Juan Gabriel, with adscription in the Instituto Tecnológico de Culiacán.and Universidad de Guanajuato, in the next Section an article* Thresholding images *by* GARCÍA-MARTÍINEZ, Manuel Darío *with adscription in the Universidad de Guanajuato, in the next Section an article* Wavelets for correction of ECG images *by AGUIRRE-RAMOS, H. with adscription in the Universidad de Guanajuato.*

Content

Article	Page
Brain tumor and vascular structures segmentation applied in computer assisted surgery	1-9
Kalman filter for skin-colored object tracking	10-15
Bayesian classification of oranges using image processing	16-20
Segmentation of vascular structures around brain tumors using region growing on Frangi vesselness	21-26
Multiumbral optimal segmentation through a metaheuristic optimization algorithm	27-31
Thresholding images	32-35
Wavelets for correction of ECG images	36-41
Instructions for Authors	
Originality Format	
Authorization Form	

December 2015 Vol.1 No.1 1-9

Brain tumor and vascular structures segmentation applied in computer assisted surgery

ILUNGA-MBUYAMBA, Elisee*† and AVIÑA-CERVANTES, J. G.

Universidad de Guanajuato, Division de Ingenierias, Campus Irapuato-Salamanca. Valle de Santiago km 3.5+1.8, Communidad de Palo Blanco, 36885 Salamanca, GTO, Mexico

Received July 17, 2015; Accepted October 20, 2015

Abstract

A possible treatment of brain tumor consists in a surgery performed by neurosurgeons who open the skull (called craniotomy). By navigating through the brain, they reach the tumor tissues and try to remove the maximum possible. The task is tricky because of the small operation field delimited by the craniotomy, also because of the difficulty to differentiate the brain healthy tissue surrounding the tumor and the brain shift that occurs. Furthermore, the use of an ultrasound contrast agent does not allow to distinguish the tumor remnant with other hyperechogenic structures after resection. An additional tool for intraoperative imaging represents therefore a crucial element to guide the navigation through the brain safely and improve the resection task.

Brain tumor, image segmentation, vascular structures, vesselness.

Citation: ILUNGA-MBUYAMBA, Elisee and AVIÑA-CERVANTES, J. G. Brain Tumor and Vascular Structures Segmentation Applied in Computer Assisted Surgery. ECORFAN Journal-Democratic Republic of Congo 2015, 1-1: 1-9

* Correspondence to Author (email: avina@ugto.mx)
† Researcher contributing first author.

Introduction

The operation involving blood vessels requires the segmentation of vascular structures in medical image (CTA, MRA, CEUS, and Color Doppler) for a good diagnostic. The extracted region can be examined by its form, its superficies or its volume in 3D. Despite remarkable efforts consented in recent years, segmentation is still one of the problem not solved in general. Radiologists and medical experts spend most of the time manually segmenting medical images. However, computational application performs the segmentation with the least possible error and in a record time. Several techniques was proposed for this purpose. The simplest approach for segmentation is the thresholding [1, 2] followed by its sophisticated version, region growing [3]. The first method suffer of many drawbacks such as: it fails in the presence of smooth edge, of varying intensity and sensible to the noise. The second one has the problems of leakage when the boundary is blurred and the difficulty to set a threshold value confining the target. To overcame the limitation of the firsts methods, several techniques are used such as hybrid genetic algorithm and Artificial Neural Network Fuzzy (ANFIS) [4] in brain tumors segmentation, graph cut with shape priors [5,6] and active contour model introduced by [7] which used an explicit type of curve representation. The level set approach [8] was proposed to address the curve parameterization issue of the last method. Vessels segmentation is achieved also by using the Hessian operator as presented in [9]. Krissian et al. proposed a model which combine the Hessian matrix and the gradient-based structure tensor [10] to get a robust technique to extract tubular structure. Several research have proposed different possibilities for the correction of brain displacement that happens during tumor resection [11-13]. In [14, 15], this problem is addressed based on vessels segmentation.

In this work, we tested different segmentation methods for the extraction of vascular structures in image data involved in tumor resection surgeries. Three applications are presented in this context, firstly, the visualization of the blood vessels in cT1MR (contrast T1-weighted MR) data for the surgery planning, secondly the brain shift evaluation and finally the vascular structure tracking in intraoperative US data. One visualization tool was implemented for this purpose to assess the correction of the brain shift, to identify the vascular structures after resection and to differentiate them with residual tumors. This report is organized as follows: section II describes the segmentation methods, in section III, the methodologies proposed and based on blood vessels segmentation are applied to medical applications.

The section IV presents the results of tests performed on the phantom and patient data set. Preceded by a discussion section, the last one concludes the analysis.

Background

A. Thesholding

The thresholding is the simplest method to partition a grayscale image into two classes. The result obtained after segmentation is called binary image. By setting a threshold value, the pixels are classified in one of the two classes as described following:

$$I_t(x,y,z) = \begin{cases} 0, & if\ I(x,y,z) < t \\ 1, & if\ I(x,y,z) > t \end{cases} \quad (1)$$

Where $I_t(x, y, z)$ and $I(x, y, z)$ represent respectively the voxels of the segmented image and those of the original image at the coordinate point (x, y, z), and t is the threshold value.

ISSN-On line: 2414-4924

B. Region Growing

The basic idea of the Region Growing Threshold method is to start the segmentation from a given seed point selected in the target to be segmented.

The object is segmented by a recursive search among the voxels in the neighborhood of the starting point to find those that meet a membership criterion to the region. Usually, the threshold value is used as a criterion of belonging to the region. The final partition segmented R is defined by the mathematical formulation:

$$\bigcup_{i=1}^{n} R_i = R$$
$$R_i \cap R_j = \emptyset$$
$$P(R_i) = True \quad (2)$$

Where Ri are the connected points satisfying the predicate P.

C. Vesselness

The use of other segmentation methods is not adequate for the segmentation of MRT data.

Usually, those models are used on angiographic data. The vesselness based Hessian matrix is useful to enhance vascular structures and to allow the visualization of vessels relative to the tumor. The method consist to extract the brain from MRT1 as preprocessing step, to segment blood vessels and the tumor. The 3D surface rendering presents all structures together, what is interesting for neurosurgeons.

The filtering based on hessian matrix allows to extract vascular structure in medical images by calculating the eigenvalues $\lambda_1, \lambda_2, \lambda_3$ $(|\lambda_1| < |\lambda_2| < |\lambda_3|)$ of $\nabla^2 I$, and the corresponding eigenvectors e_1, e_2, e_3.

$$H = \begin{bmatrix} \partial^2 I/_{\partial x^2} & \partial^2 I/_{\partial x \partial y} & \partial^2 I/_{\partial x \partial z} \\ \partial^2 I/_{\partial x \partial y} & \partial^2 I/_{\partial y^2} & \partial^2 I/_{\partial y \partial z} \\ \partial^2 I/_{\partial x \partial z} & \partial^2 I/_{\partial y \partial z} & \partial^2 I/_{\partial z^2} \end{bmatrix} \quad (3)$$

Having this eigenvalues and eigenvectors, the intensity and the direction of vascular structures can be found.

In 3D, the Hessian matrix H is composed by the second-order partial derivatives of the image I at a point (x,y,z). To control the width of the extracted centerline, the partial second derivatives of I in (3) will be replaced by the partial second derivatives of Gaussian as:

$$\frac{\partial^2 I_\sigma}{\partial x^2} = \left\{\frac{\partial^2}{\partial x^2} G_\sigma\right\} * I$$
$$\frac{\partial^2 I_\sigma}{\partial x \partial y} = \left\{\frac{\partial^2}{\partial x \partial y} G_\sigma\right\} * I$$
$$G_\sigma = \frac{1}{\sqrt{(2\pi\sigma^2)^3}} exp\left(-\frac{x^2 + y^2 + z^2}{2\sigma^2}\right) \quad (4)$$

Where $G\sigma$ is a Gaussian function with a standard deviation σ.

Using the eigenvalues, the dissimilarity measure is described as follows:

$$R_A = \frac{|\lambda_1|}{|\lambda_2|} \quad (5)$$
$$R_B = \frac{\lambda_1}{\sqrt{|\lambda_2 \lambda_3|}} \quad (6)$$
$$S = \sqrt{\sum_{i=1}^{3} \lambda_i^2} \quad (7)$$

The vesselness function can be calculated as described in [9]:

$$v_0(\sigma) = \begin{cases} 0, if\ \lambda_2 > 0\ or\ \lambda_3 > 0, \\ \left(1 - \exp\left(-\frac{R_A^2}{2\alpha^2}\right)\right) exp\left(-\frac{R_B^2}{2\beta^2}\right) \left(1 - \exp\left(-\frac{S^2}{2c^2}\right)\right), otherwise \end{cases} \quad (8)$$

ISSN-On line: 2414-4924

December 2015 Vol.1 No.1 1-9

Where α, β, and c are thresholds which control the sensitivity of the filter to the measures R, and S. By applying a multiple scales, the maximum response is the final estimate of vesselness and also the enhanced image which corresponds to line like structures.

$$v_l = \max_{\sigma_{min} \le \sigma \le \sigma_{max}} \{v_0(\sigma)\} \quad (9)$$

In this equation σ_{min} and σ_{max} values represent respectively the minimum and maximum scales wherein the structures are expected to be found.

They are chosen in order to cover the range of the vessels widths.

Methods

A. Segmentation of cerebral vascular structures driven by vesselness

Despite the contrast agent used in cT1MR data, blood vessels are still little contrasted, and othe anatomical structures are visible and represented with similar gray intensities. The segmentation becomes more complex than in CTA or MRA data, where only the vascular structures are represented.

To improve the visualization of vessels in the preoperative planning step, the vesselness method has been adopted for the segmentation task. Due to the skull noises affecting the result, a preprocessing was carried out to extract the brain using Brain Surface Extraction tool (BSE). Secondly, the vesselness was applied on the brain to enhance the visualization of vascular structures. In the method illustrated in the Fig. 1, the vesselness was performed with a single scale σ = 1 and the extracted target was filtered by a 3x3 median filter to reduce noises.

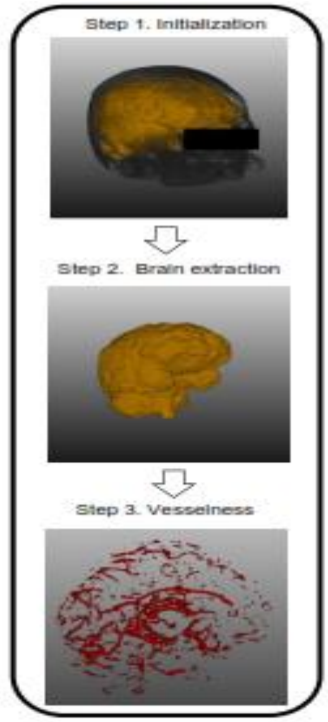

Figure 1 Image segmentation process proposed

B. Vessels-based registration for brain shift correction Since a brain displacement occurs after the craniotomy and during tumor resection, the correction of the initial registration is required. The vascular structures was used as a reference to achieve the correct alignment during surgery. The first tests have been performed on the phantom data.

With a CEUS image a little misaligned to the CT image, we used the vascular structures to perform the alignment. The method consist firstly by a segmentation of vascular structures in both modalities, and followed by a registration task of these segmented elements. The registration provided a transformation matrix that allows the overlapping of images. When this matrix is applied to the CT image, the alignment error converge to zero.

ISSN-On line: 2414-4924

The methodology for correcting the brain shift is illustrated in Fig. 2, where the segmentation in step 1 was effected with a simple thresholding method.

The registration on the second step has been performed using the Normalized Cross Correlation (NCC) as similarity measure. In the third step, the corrected alignment of the CT and CEUS images is presented. The computation iteration time was of 34.9 seconds and the images size 88, 40, 111 in 3D.

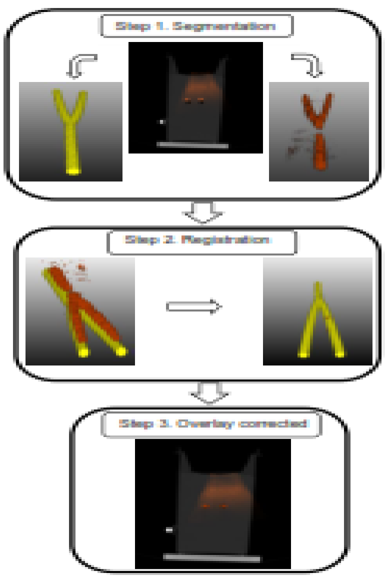

Figure 2 Proposed methodology for correcting Misalignment

This correcting process can be described as follows:

1. Manually definition of the Region of interest (ROI) on the images,
2. Define the Threshold value by the user and compute the segmentation,
3. Start the registration of the segmented structures, The similarity measure is calculated as:

$$NCC = \frac{1}{\sigma_x \sigma_y} \sum_i (x_i - \bar{x})(y_i - \bar{y}) \qquad (10)$$

4. Display the final solution

Our contribution is the evaluation of the accuracyand of the computation time relative to the shapeand the pattern size. By reducing the ROI size, the segmented structures also are reducing in order toimprove the response time of the algorithm. Thecomputation iteration time decreased to 1.2 seconds (image size: 84, 37, 34), what means 29 times fasterthan in the first case or an improvement of 96.56 percent.

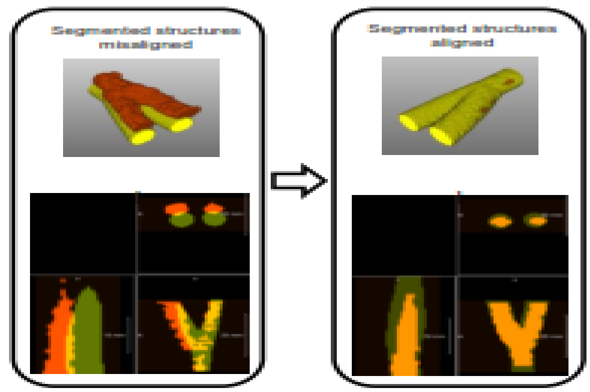

Figure 3 Overview of the computation time Improvement

The registration using small structures is computed with a reduced iteration time, and the choice of a bifurcation helps to make the algorithm robust to noises and less sensible to errors related to the confusion in identification of targets.

Given that this proposed scheme has shown its capability to remedy the misalignment of images, it have also tested on real data.

C. Tracking of vascular structures in intraoperative US

The patient image dataset includes a preoperative contrast T1 MR data and 3D intraoperative contrast enhanced ultrasound (3D-iCEUS) data acquired before and after tumor resection.

ISSN-On line: 2414-4924

The use of a contrast agent enhances the visualization not only the tumors, but also the vascular structures. On the other hand, to differentiate the remnant tumor with the blood is a complex task in CEUS after resection.

Our method proposes to track vessels in CEUS data using a pattern extracted in cT1MR data, and the identification of the vessels avoids the confusion between vessels and residual tumor in CEUS images. Therefore, with the implemented tool, the user defines a ROI in the preoperative MR data including a blood vessel perfusing the tumor to

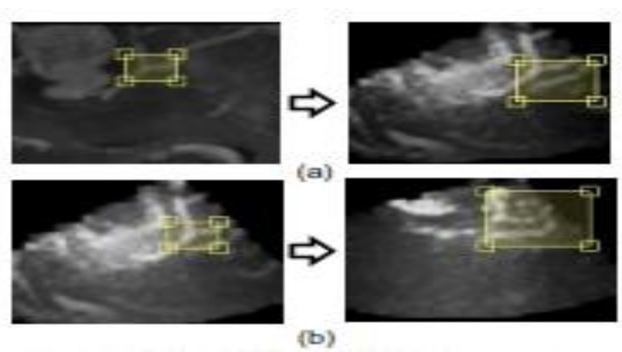

Figure 4 (a) ROI in MRT and CEUS before resection, (b) ROI CEUS before and after resection

Track the vessels intraoperatively based on the proposed methodology as shown in Figure 6 and 7.

Using a rigid registration method, the selected pattern is searched in the 3D-iCEUS data before resection within a larger region because of the brain shift (Fig. 4). The detected blood vessel becomes then the new pattern to identify the same vascular structure in the 3D-iCEUS data after resection. The extracted blood vessels are finally segmented using a vesselness method and visualized.

Results

This section shows the results obtained in each application, and the implementation was done with an Intel Celeron, 1.5 Ghz and 2 GB of memory. The algorithms have been implemented using MeVisLab tool and ITK C++ (Insight Segmentation andRegistration).

A. Visualization of blood vessels for brain tumor resection planning

The figure 5 illustrates how the vascular structures are displayed together with tumor data to facilitate the surgery planning task by the visualization. The tumor was segmented using a region growing threshold connecting.

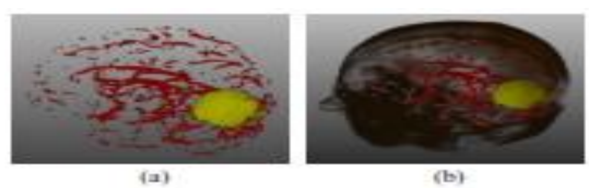

Figure 5 (a) Blood vessels image merged with a tumor, (b) Segmented structures displayed in the skull

B. Correction of the brain deformation based onvascular structures

Since the brain shift can be corrected using blood vessels, some results of the tests performed on a patient data set is presented below.

At the same position, the figure 8 (a) and (b) shows the misalignment between the MRT image and the CEUS data occurred during brain tumor resection. By applying the method of vessels-based registration to correct the brain shift, the result obtained is illustrated in the figure 8 (c).

Furthermore, in the figures 9, the first one shows the overlay of preoperative and intraoperative data when there is a brain deformation. In the second one, the result obtained by the proposed methodology is presented.

C. Blood vessel tracking in intraoperative CEUS

Our method was tested on patient data in the context of a brain tumor operation.

It was validated by registering the preoperative MR data with the 3D-iCEUS data using the transform matrix obtained in the registration method.

The correct overlapping of anatomical structures, especially the vessels, was visually checked in the 3D-iCEUS data before and after resection.

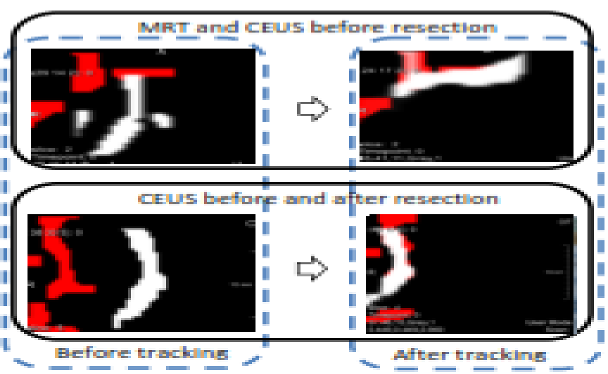

Figure 6 Tracking process flow

Discussion

Application 1: for the planning stage, the segmentation performed with the vesselness method gives an output with noises and should be validated by many specialists. The future work will be to test other vesselness method as described in [16].

Application 2: in this work, we used a rigid transformation model that allows to correct the brain shift in a local volume. Due to the elastic deformation of the brain, an elastic registration method is needed to perform the task.

Application 3: the big issue in the segmentation task in iCEUS for tracking vessels data still the quality of available data. The image quality is important in order to get an expected result with the proposed tool and method. The future work could be focused on the image quality enhancement as preprocessing step to overcome some flaws that occurred in the tracking process.

MRT and CEUS before resection
CEUS before and after resection
Before tracking
After tracking

Conclusion

Various segmentation methods are used on a patient data set in medicine. In this work, three medical applications based on segmentation of vascular structures have been presented in the context of brain tumor surgery. The obtained results indicate that the vesselness method is a suitable approach to help neurosurgeons in a planning stage of brain tumor resection. With a 3D visualization, they can choose the least invasive trajectory to reach their target. Intraoperative CEUS modality is a cheaper and easy method to check the brain deformation and to identify the tumor tissues. The use of blood vessels as a reference pattern has shown its capability to correct the misalignment of cerebral structures and to track a vessel after resection in CEUS data to differentiate it with the remnant tumor.

Acknowledgements

This work has been supported by the National Council of Science and Technology of Mexico (CONACYT) under the grant number 493442. We would like to thank CONCYTEG for the support to this work. The author would like also to thank Dr. Claire Chalopin at Innovation Center Computer Assisted Surgery (ICCAS), Universität Leipzig, and Dr. Dirk Lindner University Hospital, department of Neurosurgery, Universität Leipzig in Germany for the supervision of this work and the collection of data.

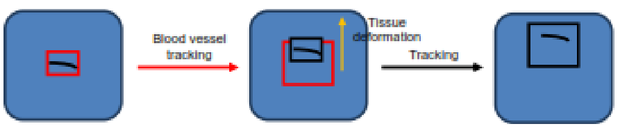

Figure 7 Tracking vessels

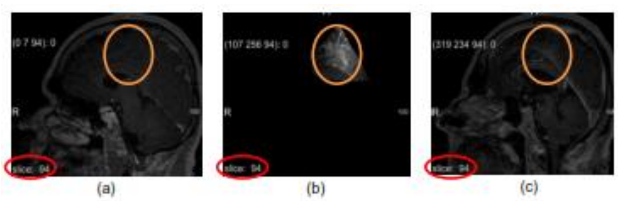

Figure 8 (a) Initial MRI data, (b) iCEUS and (c) MRI data with a brain shift corrected

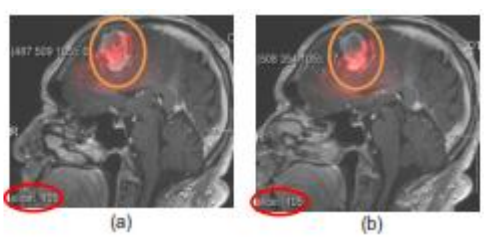

Figure 9 (a) Overlay of MRI and iCEUS data with brain deformation, (b) MRI and iCEUS data superimposed after the correction of brain shift

References

Sahoo, P. K. et al., "A survey of thresholding techniques,"Computer Vision, Graphics, and Image Processing, 41: 233260 (1988).

M. Usman Akram, Shoab A. Khan, “Multilayered thresholding-based blood vessel segmentation for screening of diabetic retinopathy”, Engineering with Computers, 2011

B. E. Chapman, J. O. Stapelton, and D. L. Parker, “Intracranial vessel segmentation from time-of-flight MRA using preprocessing of the MIP Z-buffer: accuracy of the ZBS algorithm,” Medical Image Analysis, vol. 8, no. 2, pp. 113–126, 2004.

Minakshi Sharma and Sourabh Mukharjee, “Brain Tumor Segmentation using hybrid Genetic Algorithm and Artificial Neural Network Fuzzy Inference System (ANFIS),” International Journal of Fuzzy Logic Systems (IJFLS), Vol.2, No.4, October 2012.

Hui Wang and Hong Zhang, “Adaptive shape prior in graph cut segmentation,” in proceeding of the 17th IEEE International Image Processing, (ICIP 2010), pp.3029-3032, Sept 2010.

N. Vu and B.S. Manjunath, “Shape prior segmentation of multiple objects with graph cuts”, in proceeding of IEEE Conference on Computer Vision and Pattern Recognition, (CVPR 2008), pp.1-8, June 2008.

Kass, M., Witkin, A., Terzopoulos, D.,”Snakes: Active contour models”, International Journal of Computer Vision 1(4) (1988) 321-331

Ravi Malladi, James A. Sethian, Baba C. Vemuri, “Shape Modeling with Front Propagation: A Level Set Approach”, IEEE Trans. Pattern Anal. Mach. Intell. 17(2): 158-175 (1995)

ISSN-On line: 2414-4924

Alejandro Frangi, WiroNiessen, Koen Vincken, and Max A. Viergever, “Multiscale vessel enhancement filtering”, Medical Image Computing and Computer-Assisted interventation, MICCAI 98, pages 130–137, 1998.

Krissian K, Farneback G. “Techniques in the enhancement of 3D angiograms and their applications”. In: Leondes CT, editor. Medical imaging systems technology: methods in cardiovascular and brain systems. Singapore: World Scientific Publishing 2005: 359, 396.

Olivier Ecabert, Torsten Butz, Arya Nabavi, JeanPhilippe Thiran, ”Brain Shift Correction Based on a Boundary Element

Biomechanical Model with Different Material Properties”, Medical Image Computing and ComputerAssisted interventation, MICCAI 2003, pages 41–49, 1998, 2003

Dumpuri, Prashanth; Thompson, Reid C.; Sinha, Tuhin K.; Miga, Michael I., “Automated brain shift correction using a pre-computed deformation atlas”, Medical Imaging 2006: Visualization, Image-Guided Procedures, and Display, Vol.6141, pp 430–437, 2006.

Gonzalez, J. ; Univ. of Las Palmas de Gran Canaria, Las Palmas ; Sosa-Cabrera, D.; Ortega, M. ; Gil, J.A., “P2C-3 Ultrasound Based Intraoperative Brain Shift Correction”, Ultrasonics Symposium, 2007. IEEE, pp 1571 – 1574, 2007.

Reinertsen I, Descoteaux M, Siddiqi K, Collins DL. : Validation of vessel-based registration for correction of brain shift. Med Image Anal 2007; 11: 374 – 388.

Reinertsen I, Lindseth F, Unsgaard G, Collins DL. Clinical validation of vessel-based registration for correction of brain-shift. Med Image Anal 2007; 11: 673 – 684.

Chalopin C, Krissian K, Meixensberger J, Müns A, Arlt F, Lindner D., “Evaluation of a semi-automatic segmentation algorithm in 3D intraoperative ultrasound brain angiography”, Biomedizinische Technik/Biomedical Engineering. Vol. 58, pp 293–302, May 2013.

Kalman filter for skin-colored object tracking

H.-AGUIRRE-RAMOS, J. G.†, AVINA-CERVANTES, E. and ILUNGA, Mbuyamba

Universidad de Guanajuato, Division de Ingenierias Campus Irapuato-Salamanca., Carretera Salamanca-Valle de Santiago km 3.5 + 1.8 km. Comunidad de Palo Blanco, C.P. 36885. Salamanca, Gto., Mexico.,

Received July 20, 2015; Accepted October 21, 2015

Abstract

Applying a Kalman filter, a skin-colored object is trac- king even if it is partial or total blocked. Using the EM algorithm to obtain the probability distributions for both skin and nonskin classes a naive Bayesian classifier is used to extract the current object position features, and use them as an input for the Kalman filter. Using the skin segmentation instead of the gradient differences, only skin-colored objects are tracked, preventing the tracking of undesired moving objects.

Kalman, expectation maximization, bayes, object tracking.

Citation: H.-AGUIRRE-RAMOS, J. G., AVINA-CERVANTES, E. and ILUNGA, Mbuyamba. Kalman filter for skin-colored object tracking. ECORFAN Journal-Democratic Republic of Congo 2015, 1-1: 10-15

† Researcher contributing first author.

Introduction

Object tracking is an important issue in tasks such as surveillance, biological, control or military processes and other industrial applications such as quality control or mass production. Since one scene can contain several moving objects a simple difference of gradient images can not be used if only one kind of object is required to be tracked; therefore, a more optimal solution to extract the position features is needed.

We have several feature extraction techniques available, but in this paper, the use of the naive bayesian clasifier is explored. The addition of a coste function and the combination of different features show a better performance once they are applied on the database.

Using the UC Irvine Machine Learning Repository skinnonskin database [1], a set of 183792 samples of skin and nonskin are used in the training process, while the 61265 remaining ones are used for testing purposes of the probabilistic model.

Each frame is acquire and processed with the EM modeled naive Bayesian Classifier to obtain the current location as an input to the Kalman filter wich estimate the position of the data.

The first section of this paper will introduce the problem and characteristics of the used data, the second section introduce the mathematical models to the reader. The sections three and four shown the development and experimental results of the proposed method, while the last section presents the conclusions.

Mathematical models

This section introduced the mathematical expressions for the Kalman filter, the naive Bayesian classifier and the Expectation Maximization (EM) algorithm.

For each part of the final algorithm a few considerations are taken in order to achieve the results.

A. Kalman Filter

Kalman filter is a recursive algorithm wich estimates the position and uncertainty from a moving feature in the next iteration. It is supposed that the acquisition time from each image to be analyzed is $t_k = t_0 + k\Delta T$ for $k = 1, 2, ..., n$, whit a small ΔT value.

The system is modeled using the state vector s_k defined in (1) and a set of equations called the system model. The state vector contains the position (x_k , y_k) and velocity (v^x , v^y) of the object in the instant k.

$$s_k = [x_k \quad y_k \quad v_k^x \quad v_k^y]^T \tag{1}$$

The system model uses the expression in (2), where φk 1 is called the transition matrix that may or not be time dependent wich contain the relations between the past state with the current one.

$$s_k = \phi_{k-1} S_{k-1} + \xi_{k-1} \tag{2}$$

The relations in (3) are used to define ϕ_k ; these equations lead to (4).

December 2015 Vol.1 No.1 10-15

$$\begin{aligned} x_k &= x_{k-1} + v_{k-1}^x \\ y_k &= y_{k-1} + v_{k-1}^y \\ v_k^x &= v_{k-1}^x \\ v_k^y &= v_{k-1}^y \end{aligned} \tag{3}$$

$$\begin{pmatrix} x_k \\ y_k \\ v_k^x \\ v_k^y \end{pmatrix} = \begin{pmatrix} 1 & 0 & 1 & 0 \\ 0 & 1 & 0 & 1 \\ 0 & 0 & 1 & 0 \\ 0 & 0 & 0 & 1 \end{pmatrix} \begin{pmatrix} x_{k-1} \\ y_{k-1} \\ v_{k-1}^x \\ v_{k-1}^y \end{pmatrix} + \begin{pmatrix} \xi_1 \\ \xi_2 \\ \xi_3 \\ \xi_4 \end{pmatrix} \tag{4}$$

The ξ variable represent the system perturbations due to additive noise and it is modeled as a gaussian white noise with mean zero and covariance matrix Qk

$$Q_k = \begin{pmatrix} \sigma_Q^2 & 0 & 0 & 0 \\ 0 & \sigma_Q^2 & 0 & 0 \\ 0 & 0 & \sigma_Q^2 & 0 \\ 0 & 0 & 0 & \sigma_Q^2 \end{pmatrix} \tag{5}$$

Since this filter estimate the state, it is supposed that a noisy measure is taken. This relation is shown in (6)

$$z_k = H_k s_k + \mu_k \tag{6}$$

Where zk is formed with the positions of the object measured with a sensor, but since a noisy measure is supposed, the μ component is added deriving in the following relation

$$\begin{pmatrix} z_k^x \\ z_k^y \end{pmatrix} = \begin{pmatrix} 1 & 0 & 0 & 0 \\ 0 & 1 & 0 & 0 \end{pmatrix} \begin{pmatrix} x_{k-1} \\ y_{k-1} \\ v_{k-1}^x \\ v_{k-1}^y \end{pmatrix} + \begin{pmatrix} \mu_1 \\ \mu_2 \end{pmatrix} \tag{7}$$

Where μk defines a white gaussian noise with mean zero and covariance matrix Rk

$$R_k = \begin{pmatrix} \sigma_R^2 & 0 \\ 0 & \sigma_R^2 \end{pmatrix} \tag{8}$$

Once the system is modeled the Kalman equations are applied, these equations include the estimator precovariance (9), the Kalman gain (10), the optimal state estimator (11) and the estimator covariance matrix (12).

$$P_k' = \phi_{k-1} P_{k-1} \phi_{k-1}^T + Q_{k-1} \tag{9}$$

$$K_k = P_k' H_k^T (H_k P_k' H_k^T + R_k)^{-1} \tag{10}$$

$$\hat{s}_k = \phi_{k-1} \hat{s}_{k-1} + K_k (z_k - H_k \phi_{k-1} s_{k-1}) \tag{11}$$

$$P_k = (I - K_k H_k) P_k' \tag{12}$$

B. Bayesian classifier

Is a probabilistic classifier based on two assumptions:

The decision problem can be described in probabilistic terms.

The probability for all possible values is known.

This classifier uses the Bayes theorem stated in (13).

$$P(h|D) = \frac{P(D|h)P(h)}{P(D)} \tag{13}$$

Where

h correspond to the hypothesis D is the observed data P(h) and P(D) are the probabilities of h and D independent of each other.

P(Djh), a conditional probability, is the probability of the the observed data D once the h hypothesis is accomplished.

P(hjD), is the probability of occurrence of h hypothesis given the D data.

Since P(D) is considered a constant (for all the hypothesis), it can be omitted from the decision, and then we can use the maxima a posteriori (MAP) shown in (14) or the maximum likelihood (ML) shown in (15). The use of one of other will depend in the training mode, if each hypothesis has the same occurrence probability the ML classifier is used, otherwise the MAP classifier is used.

ISSN-On line: 2414-4924

$$h_{MAP} = \arg \max P(D|h)P(h) \quad (14)$$

$$h_{ML} = \arg \max P(D|h) \quad (15)$$

C. Expectation Maximization: GMM

The EM algorithm group a data set defining the probability of each one each group, this is based on an statistic model of finite mixture of gaussian functions.

This model describe a set of k groups with a gaussian or normal probability distribution for each one. The parameters of the distributions can be calculated using the probability of belong of each data and the data itself; the equations (16) to (18) describe the calculus for the mean, the variance and the probability of each group distribution respectively, in each case, the w variables correspond to the probability of the data to belong to the current group.

$$\mu_A = \frac{\sum_{i=1}^{n} w_{Ai} x_i}{\sum_{i=1}^{n} w_{Ai}} \quad (16)$$

$$\sigma_A^2 = \frac{\sum_{i=1}^{n} w_{Ai}(x_i - \mu_A)^2}{\sum_{i=1}^{n} w_{Ai}} \quad (17)$$

$$p_A = \frac{\sum_{i=1}^{n} w_{Ai}}{\sum_{i=1}^{n} w_{Ai} + \sum_{i=1}^{n} w_{Bi}} \quad (18)$$

With an aproximation of the parameters, we can calcule an estimation to the group applying the gaussian distribution defined in (19).

$$f(x;\mu_A,\sigma_A) = \frac{1}{\sqrt{2\pi\sigma_A^2}} e^{\frac{(x-\mu_A^2)}{2\sigma_A^2}} \quad (19)$$

In order to obtain a better estimation, the weights (or belong probability) are updated using (20) and the algorithm is repeated until a stop condition is accomplished.

$$w_{Ax} = \frac{f(x;\mu_A,\sigma_A)p_A}{f(x;\mu_A,\sigma_A)p_A + f(x;\mu_B,\sigma_B)p_B} \quad (20)$$

Since the EM algorithm only estimates the values and seldom achieve total convergence two common stop conditions are used: define a number of iterations and achieve a maximum likelihood for several iterations.

The first one can lead to a bad estimation if a small number of iterations is selected, while the second one can never be achieve; for these reasons they should be used together in order to avoid nonconvergence problems and obtain the better estimation. The maximum likelihood estimator can be used with any of the equations in (21).

$$LP = \prod_i p_A P(x_i|A) + p_B P(x_i|B)$$
$$LP = \sum_i ln(p_A P(x_i|A) + p_B P(x_i|B)) \quad (21)$$

Modeling the problem

In order to avoid a dependent component color space the sRGB images should be converted into another color space, the one we propose to use is the CIE-L*a*b color space. Since we do not require the colors of the segmented area but its current position we do not need to return the results to the sRGB color space.

Therefore the full process will consist in the segmentation of the skincolored area and the application of the Kalman filter. To achieve the segmentation, a naïve Bayesian classifier is used applying the EM algorithm to obtain the model. The system is modeled using the equations describe in section II.

A. The model problems

While histogram based models are non-iterative methods, the EM needs a stop condition in order to stop the loop since the total convergence is seldom obtained, the incorrect application of this condition can derive in misclassified data.

Since the output of the EM is only an estimation of the actual solution, the parameters for each class distribution function will show an estimate behavior as well.

The better the stop condition, the better the results; but sometimes the condition is achieve while the output is far away from the actual solution and therefore a poor modeled distribution will be obtain instead.

The Figure 1 show the class assign for each training sample once a certain stop condition is achieve for the training data set, this graph entail that while one class training data is correctly assigned the other one include misclassified points, leading to a poorly classified results each time this model is used. The stop condition to avoid classification problems should be stated depending on each particular problem needs.

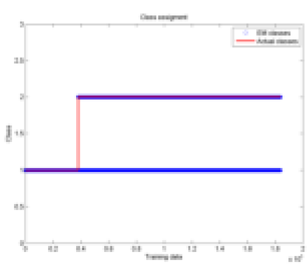

Figure 1 Convergence problem

There exist the possibility of multiple moving objects within the scene, but sometimes we will not need to track all of them; therefore we need an accurate method to detect and extract features from the desired objective.

Our selection of the Bayesian Classifier will reduce our problem to a probabilistic decision, but to choose the correct model is the real challenge.

Experimental Results

The data from Table 1 show the accuracy rate for several classifiers (Naive Bayes (Expectation Maximization with partial convergence (EM1), Expectation Maximization with total convergence (EM2) and histogrambased (Hist) pdf), Kmeans and KNN with pn rule) once they are used with CIE-L*a*b features (a component (a), b component (b), coste function (c), MatLab Gaussian fitting (f)) and the combination of them.

These results show that the use of EM algorithm outperform the classic histogram based model definition without the use of the coste function and the other two classifiers.

However, once the models are used with real data, not the one from the database, the EM models shown a better performance than the histogram based models since the first ones does not misclassify hair or clothes border pixels. In Figure 2, the versatility of the.

	Bayes			kmeans	KNN
Feature	EM1	EM2	Hist		
a	82	95.7	96.1	**93.5**	97
b	84. 2	91.7	96.7	91.9	97
ac	73.9	22.3	95.6	-	-
bc	**84.4**	22.2	96.7	-	-
ab	80.6	**98.9**	99.5	92.9	96.3
abc	79.3	23.9	**99.6**	-	-
af	82	95.7	94.3	-	-
bf	84.2	91.9	97.2	-	-
afc	73.9	22.3	21	-	-
bfc	**84.4**	22.4	53.2	-	-
abf	80.5	99	**96.9**	-	-
abfc	79.7	**99**	96.8	-	-

Table 1 Accuracy rate for different pdf models and attributes

Database and the models for segment different skin pigmentation and the problem generated for the EM convergence problem is shown.

December 2015 Vol.1 No.1 10-15

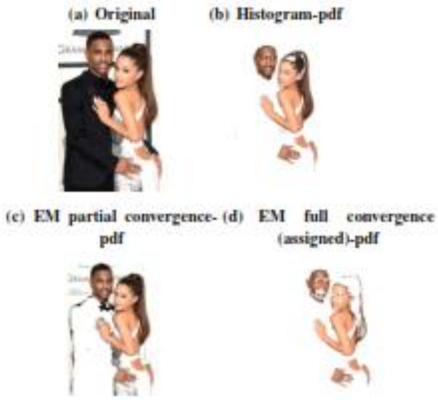

Figure 2 Skin-detection

With the features extracted, the Kalman filter can be applied. The Figure 4 contain the estimated path of a moving object once a noisy measure (current position plus white gaussian noise (N(0; 10))) is taken.

It is clear that even with a non-related initialization, the Kalman filter follow the actual path closely.

If the object is partial or total blocked the Kalman filter uses the estimation as observation and continue the process without problem.

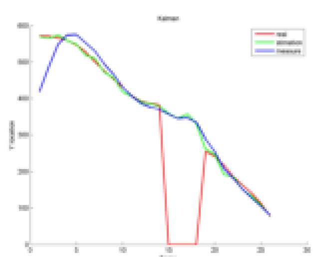

Figure 3 Kalman estimation of uncomplete data

To test the Kalman filter behavior an object is recorded on a video and its current positions based on the results of a EM modeled Bayesian classifier are obtained.

To simulate missing data the object cross behind a barrier, the results are show in Figure 4. The path in red marks the actual path of the object while the green one show the Kalman filter estimation. While we have not information of the object behind the barrier, the Kalman filter estimate its position and possible exit from it.

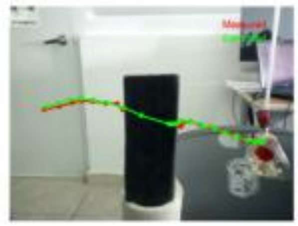

Figure 4 Kalman tracking of a total blocked object

Conclusion

EM showed a better performance than histogram based (hb) models, at least on natural images; while the hb models classify non-skin pixels with similar colors as skin ones, the use of EM assign them correctly as nonskin.

The application of the Kalman filter to found missing data showed a good performance as well, while some models consider a constant velocity, an approximate value can be found using the current and past location, solving the missing data problem and estimating a path that follows the behavior of the tracked object.

References

M. Lichman, “UCI machine learning repository,”
2013.

Bayesian classification of oranges using image processing

ILUNGA-MBUYAMBA, Elisée*† and AVIÑA-CERVANTES, Juan GABRIEL

Universidad de Guanajuato, Campus Irapuato-Salamanca.

Received July 22, 2015; Accepted October 23, 2015

Abstract

Fruits and vegetables are normally presented to consumers in batches. The homogeneity and appearance of these have significant effect on consumer decision. For this reason, the presentation of agricultural produce is manipulated at various stages from the field to the final consumer and is generally oriented towards the cleaning of the product and sorting by homogeneous categories.

The aim of this paper is to present the technique classification of oranges by vision, and to evaluate the efficiency of this technique regarding the color like quality attribute for detection of external blemishes. The segmentation procedure used, based on a Bayesian analysis, allowed to classify fruits according to their colors. The results obtained show that the quality of images to be analyzed has a great influence on the decision of the system. Blurred image increases the error of confusion in the classification, because the system will not be able to differentiate the color of good oranges with those that are rotten. For this reason it is very important to use a good quality camera providing images.

Bayesian classification, image processing, quality of fruit, segmentation.

Citation: ILUNGA-MBUYAMBA, Elisée and AVIÑA-CERVANTES, Juan GABRIEL. Bayesian classification of oranges using image processing. ECORFAN Journal-Democratic Republic of Congo 2015, 1-1: 16-20

* Correspondence to Author (email: Elise_ilunga@yahoo.fr)
† Researcher contributing first author.

Introduction

The need to measure the quality of fruits is increasing each year in industry in order to satisfy the final customers. In fruits and vegetables production lines, the quality assurance is the one of steps which is again often done manually. Orange quality assurance is done by persons trained who check the quality of fruits and classify them based on visual features. The prices of oranges are strongly related to the visual feature, for this it's one of elements very important for industry. The classification can be done in many categories, but we will consider only two in basing on the appearance, the class of healthy oranges and the class of defective oranges.

Nowadays, several manufacturers around the world produce sorting machines capable of pre- grading fruits by size, color and weight. Nevertheless, the market constantly requires higher quality products and consequently, additional features have been developed to enhance machine vision inspection systems (*e.g.* to locate stems, to determine the main and secondary color of the skin, to detect blemishes)[1].

Pattern classification deals with developing a model or method which classifies the given query data item in to one of predefined classes. A data item in most of the cases is a vector of feature values and is called a pattern. Training set is a set of patterns where for each pattern we know its class. The model or method to do pattern classification is developed by using the training set. There are various pattern classification methods, like, the Bayes classifier, nearest neighbor classifier, Perceptron, multi-layer Perceptron, support vector machines, etc.

The rest of the paper is organized as follows. Section II describes images processing and analysis by computer vision. Section III describes the system overview, Bayesian classification and color segmentation. Section IV shows results of tests. Section V gives conclusions of the project.

Image processing and analysis

Image processing and image analysis are recognized as being the core of computer vision. Image processing involves a series of image operations that enhance the quality of an image in order to remove defects such as geometric distortion, improper focus, repetitive noise, non-uniform lighting and camera motion. Image analysis is the process of distinguishing the objects (regions of interest) from the background and producing quantitative information, which is used in the subsequent control systems for decision making. Image processing/analysis involves a series of steps, which can be broadly divided into three levels: low level processing, intermediate level processing and high level processing.

Low level processing includes image acquisition and pre-processing. Image acquisition is the transfer of the electronic signal from the sensing device into a numeric form. Image pre-processing refers to the initial processing of the raw image data for correction of geometric distortions, removal of noise, grey level correction and correction for blurring. Pre-processing aims to improve image quality by suppressing undesired distortions or by the enhancement of important features of interest.

Averaging and Gaussian filters are often used for noise reduction with their operation causing a smoothing in the image but having the effect of blurring edges.

Intermediate level processing involves image segmentation, and image representation and description. Image segmentation is one of the most important steps in the entire image processing technique, as subsequent extracted data are highly dependent on the accuracy of this operation. Its main aim is to divide an image into regions that have a strong correlation with objects or areas of interest.

High level processing involves recognition and interpretation, typically using statistical classifiers or multilayer neural networks of the region of interest. These steps provide the information necessary for the process/machine control for quality sorting and grading.

The interaction with a knowledge database at all stages of the entire process is essential for more precise decision making and is seen as an integral part of the image processing process. The operation and effectiveness of intelligent decision making is based on the provision of a complete knowledge base, which in machine vision is incorporated into the computer [2].

System overview

The system that we propose will consist of three subsystems. The first one captures the orange's picture (camera), the second one processes the image and performs the classification (Image Processing and Classification), and the third one places the fruit already classified in the desired container (Healthy Output and Defect Output). This paper focuses on the classification of oranges according their appearance (healthy or defect).

Figure 1 Diagram of oranges classification process

III.1. Bayesian classification

If Ci, for i = 1,2, represents on the the two classes, and X is the feature vector extracted for the pixel whose class has to be found, then the probability that the pixel belongs to a particular class Ci is given by the posterior probability $P(Ci|X)$ of that class Ci given the feature vector X (using Bayes' Theorem):

$$P(Ci|X) = \frac{P(X|Ci)P(Ci)}{P(X)} \quad (1)$$

Where $P(Ci)$ is the prior probability of the class Ci ; $P(X|Ci)$ is the probability of feature vector X, given the pixel belongs to the class Ci ; and, $P(X)$ is the total probability of the feature vector X (i.e.,).

$$\sum_i P(X|Ci)P(Ci))$$

A Bayesian classifier first computes $P(X|Ci)$ using equation 1. Then, the classifier gives the label Cm to a given feature vector if $P(Cm |^{X_0})$ is maximal.

$Cm = \arg\max_i \{P(Ci|X)\}$. The prior probabilities $P(Ci)$, $P(X)$ and the conditional probability $P(X|Ci)$ are computed from the labeled images [4].

ISSN-On line: 2414-4924

Color segmentation and classification

The image segmentation is based on researching of areas of image with common attributes, such as brightness or texture rarely.

In this paper we focus on image segmentation (segmentation by region). Color segmentation using Bayes's theorem, specifically naive Bayes in which it is assumed that the color components (RGB) are independent. There are different methods of segmentation by region: histogram, processing by region, and by optimization. We opted for the histogram method which is simple and easy to implement. In this method, the image is decomposed into RGB and is represented by a histogram of each color. The probability that a pixel belongs to the class sought is obtained by comparing the RGB components of the image with those the database. And according to the Bayes theorem, we can take the decision that a pixel belongs to the class ω1 (healthy) or in the class ω2 (defect).

$$x \in \omega 1 \text{ , if } P(x/\omega 1) > P(x/\omega 2) \quad (2)$$
$$x \in \omega 2 \text{ , if } P(x/\omega 1) < P(x/\omega 2) \quad (3)$$

The parts of oranges with blemishes and the parts healthy are segmented according their colors, and then the percentage of each pixel classified like defective (3) or healthy (2) allows taking decision of classification of fruits. In this step we have seen that the quality of image is very important, for this reason it is important to use the high quality cameras. Also the preprocessing is necessary too for improving the quality of image, because the bad quality increases the error in classification.

Results

For experimentation we use twenty six images for healthy oranges and twenty one images for defective oranges. The image processing and classification give a satisfying result, and then this output classification should help to separate the healthy oranges with the defective in the production line.

Classified like healthy

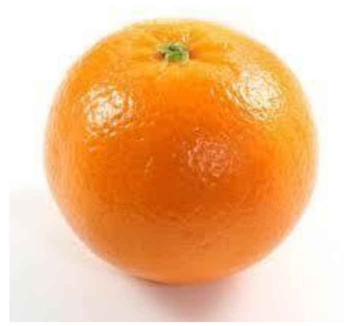

Figure 1 Image of classification orange healthy

Classified like defect

Figure 2 Image of classification orange defective

As illustrated in Figure 1, the classification is fine for healthy output, and in the Figure 2 we illustrate the classification of defective orange. In this case we choose the color background white, with this we use segmentation directly without eliminate the background. The color of background is constant, but the colors of fruits are variables in the segmentation process.

Conclusions

The segmentation method is fast and appropriate for on-line processes, but depends much on the color of the objects to be inspected. For this reason, the system needs to be trained frequently by an expert operator. The non-destructive nature of this technique, the speed and hygienic inspection condition help to maintain its attractiveness for application in the food industry.

Our system showed good results when positioning of oranges facilitate detection of blemishes on the skin. For this reason we recommend using more cameras to take many images in different angles, for tracking blemishes on the oranges skin.

We had a classification error of 2%, it means that 1 orange was classified like defective but it was healthy. And we obtained 98% of correct classification. With the technique of Kernel Density we improve the classifier by reducing the classification error to almost zero.

References

1 J. Blasco, N. Aleixos, Machine Vision System for *Automatic Quality Grading of Fruit*, Spain, 2003.

2 Tadhg Brosnan, Da-Wen Sun, *Improving quality inspection of food products by computer vision*, Irland, 2003

3 Gunasekaran, S. Computer vision technology for food quality assurance. *Trends in Food Science and Technology*, 1996.

4 D. Goswami, S. Kalkan, *Bayesian Classification of Image* Structures, Germany

5 Erik G. Learned-Miller, *Supervised Learning and Bayesian Classification*, Amherst, 2011

ISSN-On line: 2414-4924

Segmentation of vascular structures around brain tumors using region growing on Frangi vesselness

ILUNGA-MBUYAMBA, Elisee*†, AVIÑA-CERVANTES, Juan Gabriel and AGUIRRE-RAMOS, Hugo

Universidad de Guanajuato, Division de Ingenierias, Campus Irapuato-Salamanca, Carretera Salamanca. Valle de Santiago km 3.5+1.8, Communidad de Palo Blanco, 36885 Salamanca, GTO, Mexico

Received July 28, 2015; Accepted October 27, 2015

Abstract

A segmentation of 3D vascular structures based on vesselness associated with a region growing algorithm is presented in this paper. The blood vessels segmentation is still important in the diagnosis of diseases related to their forms, surfaces and volumes. The extraction of vascular structures is commonly achieved with angiographic data set, but our contribution in this work is to perform this task with standard available data in the context of brain tumor. This is a big challenge because of the variation of pixels intensity and the low contrast in cT1MR (contrast T1 Magnetic Resonance). We propose a method starting by the enhancement of tubular structures using a vesselness filter, and then the region growing algorithm is performed slice by slice in a 3D volume defines by a ROI (Region Of Interest) for segmenting blood vessels.

Brain tumor, Image segmentation, Region Growing, Vascular structures, Vesselness.

Citation: ILUNGA-MBUYAMBA, Elisee, AVIÑA-CERVANTES, Juan Gabriel and AGUIRRE-RAMOS, Hugo. Segmentation of vascular structures around brain tumors using region growing on Frangi vesselness. ECORFAN Journal-Democratic Republic of Congo 2015, 1-1: 21-26

* Correspondence to Author (email: shelin70@hotmail.com)
† Researcher contributing first author.

December 2015 Vol.1 No.1 21-26

Introduction

The analysis of vascular structures in medical image is useful in the diagnostic process of specific diseases or in the planning of surgeries with the goal to keep them intact. The segmented vessels can be used directly by surgeon for a checking or for other purposes such as registration carried out with vessels as landmarks. Despite remarkable efforts developed in recent years, medical image segmentation is still one of the problem not solved in general, because there are difficulties due to low contrast, noise, and other imaging ambiguities [1]. Radiologists and medical experts spend most of the time segmenting manually medical images. Moreover, the final result is affected by the user fatigue or missing manual steps. Several techniques were introduced to automate the process in order to handle a large number of cases with the same accuracy and high speed.

The simplest approach for segmentation is the thresholding [2, 3], but there are also improved method such as region growing [4]. The first method suffer of many drawbacks such as: it fails in the presence of smooth edge, varying intensity and sensible to the noise. The second one has the problems of leakage when the boundary is blurred and the difficulty to set a threshold value confining the target. Other techniques are used for this purpose such as hybrid genetic algorithm and Artificial Neural Network Fuzzy (ANFIS) [5] in brain tumors segmentation, graph cut with shape priors [6, 7] and active contour model introduced by [8] which used an explicit type of curve representation.

The level set approach [9] was proposed to address the curve parameterization issue of the last method.

Vessels segmentation also can be achieved with vessel enhancement filters by using the Hessian operator as presented by Frangi [10] and by Krissian et al. [11]. Krissian proposed a model which combine the Hessian matrix and the gradient based structure tensor to get a robust technique to extract tubular structures [12].

In this work, we developed a visualization tool to enhance the blood vessels in 3D MR data during brain tumor surgery with the goal to keep them intact. Tumor resections are commonly guided using a navigation system based on contrasted cT1MR data. The contrast agent highlights the brain tumor and the vascular structures as well. Especially those around the brain tumor are of interest for the surgeon. However, these blood vessels are thin and few contrasted. We tested therefore a vessel enhancement filter known as Frangi vesselness will be associated with a region growing algorithm to enhance the vascular structures in order to increase the contrast between vascular structures with other anatomical structures. The pixel intensity obtained after the vesselness is suitable for an automatic thresholding using Otsu method. This paper is organized as follows: section II describes the algorithm used for blood vessels segmentation and the proposed methodology to extract vessels around brain tumors is explained in section III. Preceded by the results section of tests performed on the patient data, the last one concludes the analysis.

Background

Region Growing

The basic idea of the Region Growing method is to start the segmentation from a given seed point selected in the target to be segmented.

ISSN-On line: 2414-4924

The object is segmented by a recursive search among the voxels in the neighborhood of the starting point to find those that meet a membership criterion to the region. Usually, the threshold value is used as a criterion of belonging to the region. The final partition segmented R is defined by the mathematical formulation:

$$\begin{aligned} &\bigcup_{i=1}^{n} R_i = R \\ &R_i \cap R_j = \emptyset \\ &P(R_i) = True \\ &P(R_i \cup R_j) = false \end{aligned} \tag{1}$$

Where Ri is the connected points satisfying the predicat P.

Vesselness

The use of other segmentation methods is not adequate for the segmentation of cT1MR data. Usually, they are used on angiographic data. The vesselness based Hessian matrix is useful to enhance vascular structures and to allow the visualization of vessels relative to the tumor.

The filtering based on hessian matrix allows to extract vascular structure in medical images by calculating the eigenvalues $\lambda 1$, $\lambda 2$, $\lambda 3$ ($|\lambda 1| < |\lambda 2| < |\lambda 3|$) of $\Delta 2$ I, and their corresponding eigenvectors e_1, e_2, e_3.

$$H = \begin{bmatrix} \frac{\partial^2 I}{\partial x^2} & \frac{\partial^2 I}{\partial x \partial y} & \frac{\partial^2 I}{\partial x \partial z} \\ \frac{\partial^2 I}{\partial x \partial y} & \frac{\partial^2 I}{\partial y^2} & \frac{\partial^2 I}{\partial y \partial z} \\ \frac{\partial^2 I}{\partial x \partial z} & \frac{\partial^2 I}{\partial y \partial z} & \frac{\partial^2 I}{\partial z^2} \end{bmatrix} \tag{2}$$

Having this eigenvalues and eigenvectors, the intensity and the direction of vascular structures can be found.

In 3D, the Hessian matrix H is composed by the second order partial derivatives of the image I at a point (x, y, z).

To control the width of the extracted centerline, the partial second derivatives of I in (2) will be replaced by the partial second derivatives of Gaussian as:

$$\begin{aligned} \frac{\partial^2 I_\sigma}{\partial x^2} &= \left\{ \frac{\partial^2}{\partial x^2} G_\sigma \right\} * I \\ \frac{\partial^2 I_\sigma}{\partial x \partial y} &= \left\{ \frac{\partial^2}{\partial x \partial y} G_\sigma \right\} * I \\ G_\sigma &= \frac{1}{\sqrt{(2\pi\sigma^2)^3}} \exp\left(-\frac{x^2+y^2+z^2}{2\sigma^2}\right) \end{aligned} \tag{3}$$

Where G_σ is a Gaussian function with a standard deviation σ.

Using the eigen values, the dissimilarity measure is described as follows:

$$R_A = \frac{|\lambda_1|}{|\lambda_2|} \tag{4}$$

$$R_B = \frac{\lambda_1}{\sqrt{|\lambda_2 \lambda_3|}} \tag{5}$$

$$S = \sqrt{\sum_{i=1}^{3} \lambda_i^2} \tag{6}$$

The vesselness function can be calculated as described in [10]:

$$v_o(\sigma) = \begin{cases} 0 & if\ \lambda_2 > 0\ or\ \lambda_3 > 0 \\ (1 - \exp(-\frac{R_A^2}{2\alpha^2}))\exp(-\frac{R_B^2}{2\beta^2}) & \\ (1 - \exp(-\frac{S^2}{2c^2})), & otherwise \end{cases} \tag{7}$$

Where α, β, and c are thresholds which control the sensitivity of the filter to the measures R_A, R_B, and S. By applying a multiple scales, the maximum response v_I is the final estimate of vesselness and also the enhanced image which corresponds to line like structures.

$$v_I = \max_{\sigma_{min} \leq \sigma \leq \sigma_{max}} v_o(\sigma) \tag{8}$$

In this equation σ_{min} and σ_{max} values represent respectively the minimum and maximum scales wherein the structures are expected to be found.

ISSN-On line: 2414-4924

They are chosen in order to cover the range of the vessels widths.

Methods

The low contrast in MR images does not facilitate the segmentation task in medical application. By using the simple region growing, the result obtained is not adequate because of the leakage in the segmentation due to the close intensity value of vessels and other structures. On the other hand, this technique is more sensitive to the initialization seed point and without an appropriate choice of this starting point, the extraction of the target fails. Because the segmentation carried out by a region growing method is based intensity, the optimal threshold value that could be chosen will extract inappropriate structures such as head bones and soft tissues. To overcome this drawback we propose first to enhance de vascular structures with a Frangi vesselness filter. Based on eigenvalues of the Hessian matrix, the filter will find the vesselness maximum response which corresponds to the tubular forms in the image. The goal of this step is to highlight the vessels in comparison with other structures. With an improved contrast between our target structures with others, an automatic thresholding algorithm such as the Otsu technique could be used to perform the segmentation. By assuming that the image to be thresholded contains two classes of pixels, the algorithm calculates the optimum threshold for separating them in order to minimize the intraclass variance and to maximize the interclass variance.

The proposed segmentation methodology, allows not only extract the vascular structures, but also our approach presents the result in a 3D model for a good evaluation.

For a 3D model, a centerline is calculated as local maximal distances for getting skeletons presented in Figure 1.

Results

The results of the proposed method are illustrated in this section. The implementation was done with an Intel Celeron, 1.5 Ghz and 2 GB of memory using Mevislab tool.

Figure 1 Skeletons

An accurate segmentation carry out manually that could be considered as reference becomes more difficult in the 3D images used. With a goal to extract vessels among different structures, our results were validated by experts based on a visual inspection as described in [13]. Fig .2(a) and Fig .3(a) show the slices of a region of interest from a cT1MR images with blood vessel to be segmented and located in the neighbour of the brain tumor. In the Fig .2(b) and Fig .3(b) the results obtained with our segmentation method are presented.

The task has been carried out with a multi scale vesselnes to extract vascular structures in the image slices. We choose $\sigma = [1, 3]$ for the first case, $\sigma = [1, 2]$ for the second case and the number of scales equal to 3 in the both cases.

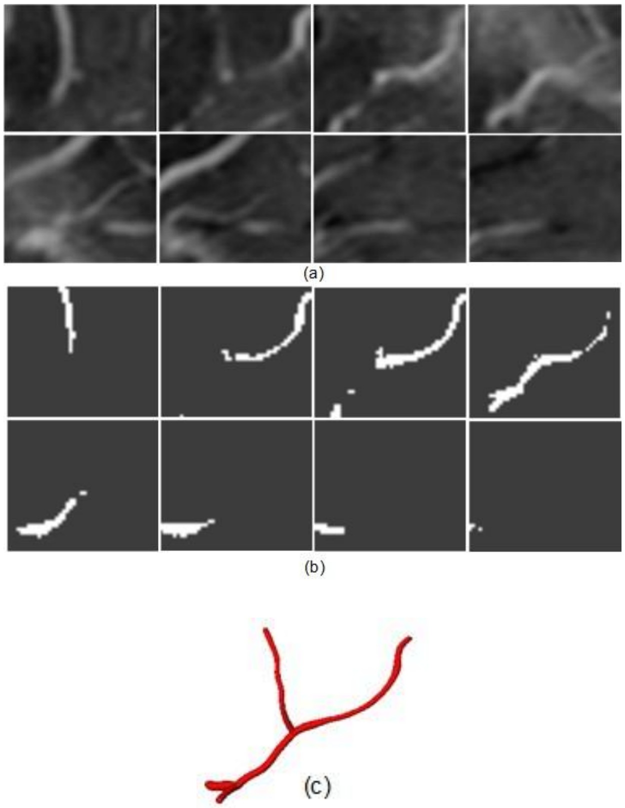

Figure 2 (a) 4 slices of a MR image with blood vessels, (b) The result segmentation of vascular structures in (a), (c) representation of the segmented vessel from the set of 8 previous slices

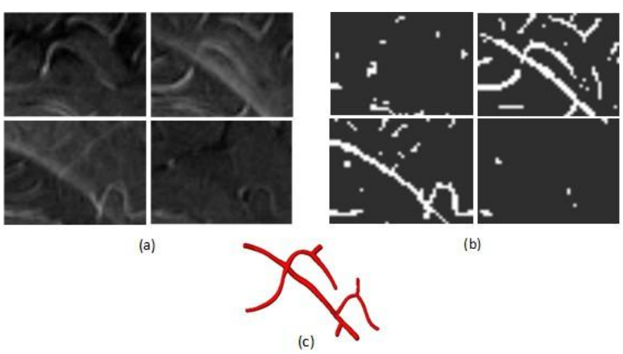

Figure 3 (a) 8 slices of a MR image containing blood vessels, (b) The result segmentation of vascular structures in the image slices (a), (c) representation of the segmented vessel from the set of 8 previous slices

Conclusion

In this paper a region growing method applied to Frangi vesselness is proposed in the context of segmentation of vascular structures around the tumor. Despite the difficulty of using this kind of data not oriented vessels visualization, the results of the proposed method have shown the capability to enhance and extract vascular structures. The 3D reconstruction is a suitable mean for surgeon in the planning step or during brain tumor surgery when the risk of damaging blood vessels should be reduced.

Acknowledgments

This work has been supported by the National Council of Science and Technology of Mexico (CONACYT) under the grant number 493442. We are also thankful to the CONCYTEG and the Programa Integral de Fortalecimiento Institucional 2012 (PIFI-2012) for their support to this work. The authors would like to thank the University Hospital, department of Neurosurgery, University of Leipzig in Germany for the collection of data.

References

1 Sharma, N., Aggarwal., L.M.: Automated medical image segmentation techniques.
J Med Phys. (2010) 3–14

2 Sahoo, P.K.e.a.: A survey of thresholding techniques. In: Computer Vision, Graphics, and Image Processing, 41. (1988) 233–260

3 M. Usman Akram, S.A.K.: Multilayered thresholding based blood vessel segmentation for screening of diabetic retinopathy. Engineering with Computers (2011)

4 B. E. Chapman, J.O.S., Parker, D.L.: Intracranial vessel segmentation from time of flight mra using preprocessing of the mip z-buffer: accuracy of the zbs algorithm. Medical Image Analysis, vol. 8 (2004) 113–126

5 Sharma, M., Mukharjee, S.

6 Wang, H., Zhang, H.: Adaptive shape prior in graph cut segmentation. in proceeding of the 17th IEEE International Image Processing, (ICIP 2010) (0) (2010)
3029 – 3032

7 Vu, N., Manjunath, B.: Shape prior segmentation of multiple objects with graph cuts. In: in proceeding of IEEE Conference on Computer Vision and Pattern Recognition, (CVPR 2008). (2008) 1–8

8 Kass, M., Witkin, A., Terzopoulos, D.: Snakes: Active contour models. Interna- tional Journal of Computer Vision (4) (1988) 321–331

9 Ravi Malladi, James A. Sethian, B.C.V.: Shape modeling with front propagation: A level set approach. IEEE Trans. Pattern Anal. Mach. Intell. 17(2) (1995) 158–
175

10 Alejandro Frangi, WiroNiessen, K.V., Viergever, M.A.: Multi scale vessel enhance ment filtering. Medical Image Computing and Computer Assisted intervention, MICCAI 98 (1998) 130–137

11 In: Medical imaging systems technology: methods in cardiovascular and brain systems. (2005)

12 Chalopin C, Krissian K, M.J.M.A.A.F.L.D.: Evaluation of a semi-automatic segmentation algorithm in 3d intraoperative ultrasound brain angiography. Biomedizinische Technik/Biomedical Engineering (2013) 293 – 302

13 Guido Gerig, Matthieu Jomier, M.C.: Valmet: A new validation tool for assessing and improving 3d object segmentation. Medical Image Computing and Computer Assisted Intervention, MICCAI 2001 (2011) 516–523

Multiumbral optimal segmentation through a metaheuristic optimization algorithm

MONTOYA-AGUILAR, Merary´*†, CRUZ-DUARTE, Jorge Mario´´ and AVIÑA-CERVANTES, Juan Gabriel´´

´Instituto Tecnológico de Culiacán.
´´Universidad de Guanajuato.

Received July 28, 2015; Accepted October 27, 2015

Abstract

Thresholding is a segmentation technique widely used in industrial applications. It is used when there is a clear difference between the objects to be extracted on the merits of the scene. While there are different methods to find a threshold, most of them do not work well when working with images of the real world due to the presence of noise levels histograms or inadequate lighting**.**

Optimal, Segmentation, Metaheuristic, Optimization, Algorithm.

Citation: MONTOYA-AGUILAR, Merary, CRUZ-DUARTE, Jorge Mario and AVIÑA-CERVANTES, Juan Gabriel. Multiumbral optimal segmentation through a metaheuristic optimization algorithm. ECORFAN Journal-Democratic Republic of Congo 2015, 1-1: 27-31

* Correspondence to Author (email: merary_girl@hotmail.com)
† Researcher contributing first author.

Introduction

Thresholding is a segmentation technique widely used in industrial applications. It is used when there is a clear difference between the objects to be extracted on the merits of the scene. While there are different methods to find a threshold, most of them do not work well when working with images of the real world due to the presence of noise levels histograms or inadequate lighting. By contrast, the method of Otsu is one of the best methods of selecting threshold for real-world images.

On the other hand, the Bat Algorithm (BA) is a metaheuristic algorithm which is inspired by the echolocation behavior of bats, and uses a frequency balance and automatic tuning of exploration and exploitation by controlling loudness and rates pulse emission. The ability of echolocation in bats is fascinating as these can find their prey and distinguish different types of insects even in complete darkness.

Statement Problem

In the last hundred years many branches of knowledge have been favored with the advent of computer equipment robust and inexpensive. One example is medicine, where it has reduced the mortality rate due to an erroneous clinical diagnosis. Being specific, the digital medical image processing prevents misplaced interpretations by specialized personnel, mostly caused by noise or scanning errors. Among the most interesting medical imaging scans as lie-rays, ultrasound and encefalografías, besides the images of electrophoresis.

Now, one way to prevent these medical problems, is to segment the images as to clarify the relevant information they contain. For this Otsu's method is traditionally used, among others.

However, this strategy does not deeply studied for more than a threshold segmentation. Thus, for each medical image, you must determine the optimal thresholds that result in the best image segmentation.

Therefore, this research intends to conduct a preliminary study of an unconventional method optimization, as an alternative strategy to the traditionally used to find the optimal thresholds in Otsu method for applications in medical imaging.

Methodology

To carry out this research was carried out the procedure described below. First, we selected, studied and implemented unconventional method optimization, metaheuristic, the virtual bat (or BA, its acronym in English Bat Algorithm). To do a commercial numerical computing platform operating on Microsoft ™ Windows 8.1® operating system used. Next, the algorithm performance tests were conducted using standard test functions commonly used in the literature. Then, as the main part of the research problem, the BA method for solving problems of image segmentation test was implemented. Each test was repeated for about 10 times, from a statistical analysis, adjust the control parameters of the method for thresholding problems. An example of these is shown in Figure 1. And the results were compared with those obtained by the method of particle swarm (or PSO, its acronym in English Particle Swarm Optimization).

Figure 1 Image Standard Test: Lena in (a) color and (b) grayscale. RESULTS

In Table 1, the original image is displayed in grayscale Lena (Figure 1), and the results obtained after a process of segmentation algorithms using unconventional optimization, BA and PSO.

In Table 1, for only a threshold, you may notice that the image treated with PSO algorithm takes pixels that should be considered in the first (lighter) region. Additionally, this happens with part of his face and arm, that is, taking part of the skin as if it belonged to the region of the hair. Therefore, it is possible to observe as part of hair which falls on the shoulder of Lena, is not separated from the rest as in the original image; so it follows that no loss of information in this region. Instead, the image obtained using BA displays more details that are clearly differentiate hair from the skin. Also, it notes that the product image is more like BA the original image.

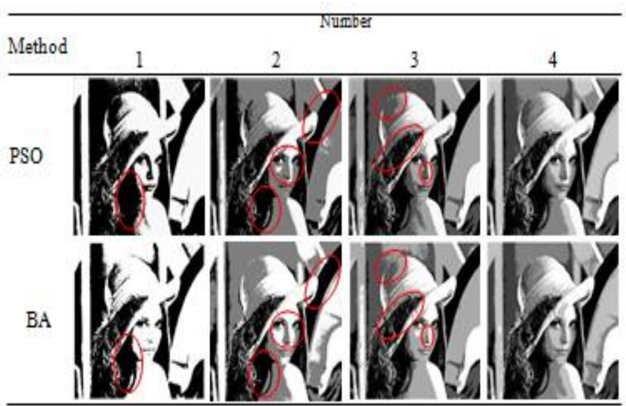

Table 1 Comparison of images with the optimal thresholds found with PSO and BA.

However, when the threshold number two, mainly noticing the arch at the bottom of the image obtained with BA are more detailed than the image achieved by PSO; in which only a single black color is observed. According to the above, emphasis is placed on that part of the hair that falls on the shoulder has higher resolution (more delineated a border), the eyes are more delineated and can more easily differentiate the rest of the face nose.

Next, for three thresholds, also in Table 1, it is observed that the hat BA image is completely separate from the background image, while image PSO thereof is mixed with the background. Also, you may notice more details in the decoration of the hat (more clearly) and nose. Finally, the images are formed from four thresholds, it appears that obtained by BA presents more details, less noise, more clearly and also the edges are outlined in greater proportion than found with PSO.

Meanwhile, in addition the above analysis, in Table 2 the thresholds found for every optimization method are presented. In this it shows that the algorithm achieved a virtual bat higher interclass variance (or objective function), which, in short, makes their results are higher quality than those determined with PSO. Additionally, by way of illustrative example, in Figure 2 the resulting histograms after segmentation process thresholds 2 and 4 are shown.

Method	1	2	3	4
		Value		
PSO		68;148	58;108;162	52;112;138;172
BA	117	93;150	80;126;170	76;114;144;180
		Function Value		
PSO		1923,04	1924,00	1924,11
BA	1601,23	1961,82	2128,31	2191,74

Table 2 Values obtained for the thresholds and the objective function with PSO and BA.

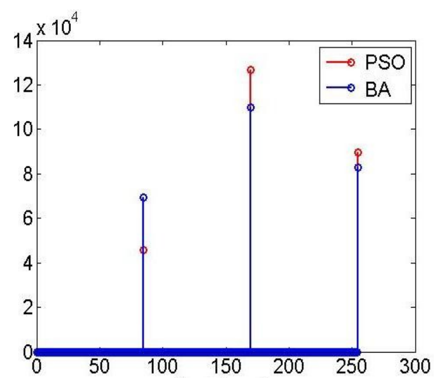

ISSN-On line: 2414-4924

December 2015 Vol.1 No.1 27-31

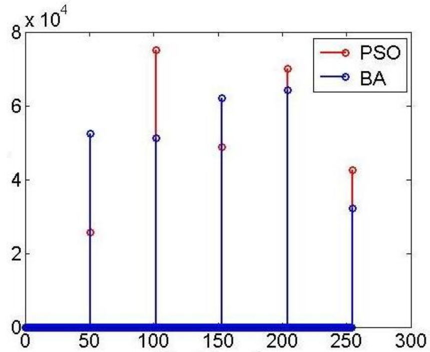

Figure 2 Histogram of the image of Lena segmented with (a) two and (b) four thresholds.

After contrast the two methods of optimization using the image traditionally used, Lena, the same procedure was implemented with a photograph taken recently by NASA, ie Pluto. In Figure 3 the original image used, and the resulting image segmentation process four thresholds with BA is shown. This is presented in Figure 4, where the histogram of the original image and optimal thresholds found by the algorithm shown virtual bat.

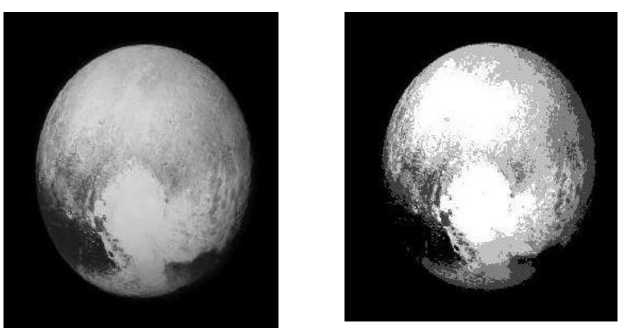

Figure 3 Image (a) the original grayscale and (b) segmented Pluto, taken from POT.

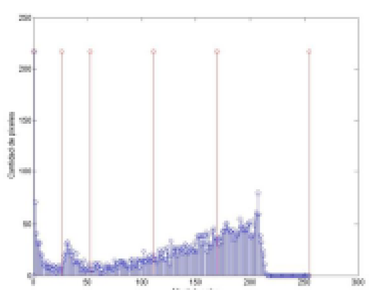

Figure 4 Histogram of the original image of Pluto and optimal thresholds obtained with BA.

Finally, an example of application to medical imaging are presented in Figure 5. In (a) and 5 (c) the two original figures used are shown, and Figures 5 (b) and 5 (d) are images resulting after optimal segmentation process through BA. In the latter, using four thresholds, details which facilitate the diagnosis by the medical staff are perceived. Therefore, the algorithm virtual bat is adequate and high potential for medical imaging tool.

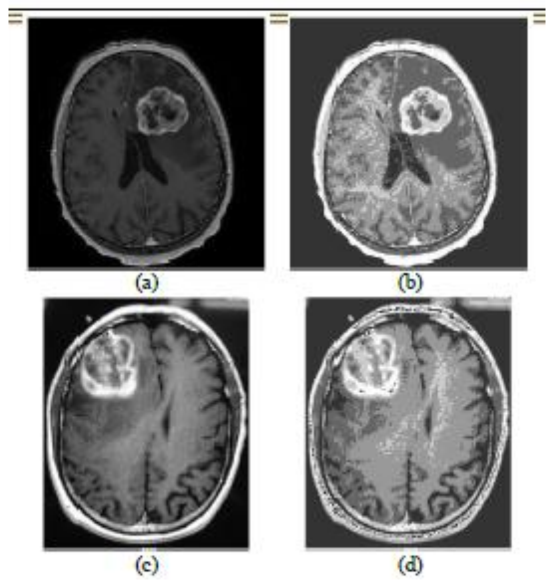

Figure 5 Original images (a) and (c), and segmented images, (c) and (d) two electroencephalograms.

Conclusions

In this paper the possible application of an alternative non-conventional optimization algorithm is explored, as is the virtual bat algorithm (BA) for the digital medical imaging through a process of multi-threshold segmentation. The first part of this work consisted of adjusting the parameters of the BA control method for subsequent implementation in image segmentation standard test. For this utility function used as the interclass variance, given by the method of Otsu.

ISSN-On line: 2414-4924

After the adjustment, the results obtained with BA and PSO segmentation of test images were compared. With the above, it was determined that the bat algorithm provides more detailed segmentation than those determined by the method of particle swarm; showing an increase of 2, 10 and 12% in the utility function 2, 3 and 4 thresholds, respectively. Then, the same procedure for other images was implemented by way of example, ie Pluto, and thus show the validity of the method. Finally, two medical images related to an anonymous patient encephalopathy were segmented. In the resulting images they were observed some subtle details in the original image, which could help in the corresponding medical diagnosis. Thus, this work found that virtual bat algorithm is a powerful tool and alternative for applications multiumbral image segmentation, especially for the case of medically related.

References

Yáñez, E. C. (2015). El algoritmo "Artificial Bee Colony"(ABC) y su uso en el Procesamiento digital de Imágenes. *Inteligencia artificial: Revista Iberoamericana de Inteligencia Artificial*, *18*(55), 50-68.

Gordón Garcés, A. M., & Constante Prócel, P. N. (2015). *Diseño e implementación de un sistema de visión artificial para clasificación de al menos tres tipos de frutas* (Doctoral dissertation, Quito, 2015.).

García Delgadillo, M. A., & Montoya Raya, B. A. (2015). SISTEMA DE VISIÓN ARTIFICIAL PARA EL MONITORE DE LOS MOVIMIENTOS INVOLUNTARIOS DEL OJO.

Alsmadi, M. K. (2015). MRI Brain Segmentation Using a Hybrid Artificial Bee Colony Algorithm with Fuzzy-C Mean Algorithm. *Journal of Applied Sciences*,*15*(1), 100.

Mesejo, P., Valsecchi, A., Marrakchi-Kacem, L., Cagnoni, S., & Damas, S. (2015). Biomedical image segmentation using geometric deformable models and metaheuristics. *Computerized Medical Imaging and Graphics*, *43*, 167-178.

Can, U., & Alatas, B. (2015). Physics Based Metaheuristic Algorithms for Global Optimization. *American Journal of Information Science and Computer Engineering*, *1*(3), 94-106.

Chandra, S., & Bhattacharyya, S. (2015). Quantum Inspired Swarm Optimization for Multi-Level Image Segmentation Using BDSONN Architecture.*Handbook of Research on Swarm Intelligence in Engineering*, 286-326.

Wang, G. G., Gandomi, A. H., & Alavi, A. H. (2015). Study of Lagrangian and Evolutionary Parameters in Krill Herd Algorithm. In *Adaptation and Hybridization in Computational Intelligence* (pp. 111-128). Springer International Publishing.

ISSN-On line: 2414-4924

Thresholding images

GARCÍA-MARTÍINEZ, Manuel Darío *†

Universidad de Guanajuato. División de Ingenieríıas Campus Irapuato-Salamanca.

Received July 29, 2015; Accepted October 29, 2015

Abstract

In this practice the implementation of a global thresholding algorithm and two local thresholding algorithms shown. In both groups of algorithms threshold values are dynamic, automatically calculated by the program in each iteration.

Thresholding, images.

Citation: GARCÍA-MARTÍINEZ, Manuel Darío. Thresholding images. ECORFAN Journal-Democratic Republic of Congo 2015, 1-1: 32-35

* Correspondence to Author (email: md.garciamartinez@ugto.mx)
† Researcher contributing first author.

December 2015 Vol.1 No.1 32-35

Introduction

Necessary to perform thresholding on images given functions were implemented. The implementation is in C, using the Open CV library, which provides a lot of useful functions for image manipulation. The first algorithm is global whose threshold is calculated using the cumulative histogram. The second algorithm is the local umbralizador Niblack [1], which uses a Local thresholding using square windows, and measures statistical used to calculate the threshold of each region. And finally, Bernsen algorithm [2] which was implemented as of Niblack uses the windows but this simply uses the maximum and minimum values of each window to determine a threshold in contrast.

Methodology

Three processing algorithms is performed on a converted image to grayscale, to this Equation 1 is used.

$$Y = 0{,}3\mathrm{R} + 0{,}59\mathrm{G} + 0{,}11\mathrm{B} \qquad (1)$$

II-A. Global thresholding

The first algorithm is described below:

Get the histogram of the gray scale image.

Obtain the cumulative histogram.

Find the gray level value for which the cumulative histogram is 0.5 and assign the threshold *th*.

The pixels with higher intensities to paint *th* white and pixels with lower intensities are painted black.

Global multilevel thresholding

The global optimization algorithm was implemented for a multilevel thresholding, ie, more than a threshold. The procedure is quite similar to the previous, but now thi N values are calculated. The calculation of the threshold values given by the Equation n2, where i runs from 1 to N - 1.

$$thi = i/N \qquad (2)$$

Local thresholding Niblack

For the second algorithm must travel the image pixel by pixel with a square window (see Figure 1). In the case of the algorithm implemented it has a resizable window. The threshold value th is calculated with Equation 3 where μ is the mean of the window, a parameter k is usually equal to 0.2 for clear images and -0.2 for dark images, and σ is the standard deviation of the window. If the value of the center pixel is greater than TH, the pixel is painted white, otherwise it is painted black.

$$th = \mu + k\sigma \qquad (3)$$

0	255	200
0	10	100
10	35	20

Figure 1 3x3 window. The center pixel is being evaluated, but using as a reference all the pixels around it.

There is a slight variation to the algorithm by adding another parameter c which suggested value is 1.3, so the formula is as in Equation 4.

$$th = \mu + k\sigma - c \qquad (4)$$

ISSN-On line: 2414-4924

December 2015 Vol.1 No.1 32-35

Local Umbralizador of Bernsen

Bernstein algorithm also occupies a window, as for the previous case was implemented resizable. For this algorithm you have two values, a local contrast (see Equation 5) and a contrast threshold. The contrast threshold has a value of 15 suggested by the author, but can receive any nonzero value. Besides, it is necessary to calculate an average gray value (Equation 6).

Local Contrast = *max* - *min* (5)

half gray = (*max* - *min*) / 2 (6)

1) Algorithm:

If the Local contrast <Contrast threshold.

- If the average gray ≥ 128, the pixel is white.
- If the above condition is not met the pixel is black.

If the local contrast contrast threshold ≥

- If the average value of the center pixel gray ≥, the pixel is white.
- If the above condition is not met the pixel is black.

Results

The test images were obtained from the database provided in reference [3].

Global thresholding

The global thresholding results are shown in Table I. The tests for different levels of shrinkage are shown.

Thresholding Niblack

Different tests for different window sizes on Niblack thresholding algorithm is performed (see Table II). Tests were performed by changing the input para'metros but are not reported due to the large number of possible combinations, but the observations are discussed in the concluding section.

Thresholding Bernsen

Different tests for different window sizes on Bernsen thresholding algorithm (see Table III) were performed. Tests were performed changing the contrast threshold. The results reported to us, but the observations are discussed in the concluding section.

Table IV a visual comparison of the performance of the three algorithms analyzed in this report is shown.

Conclusions

Visually, to test cases the results are better with global thresholding. Local thresholding with small windows have a performance that even resembles edge detectors, but noisy in areas of almost constant color, this due to slight changes in color between pixels although the human eye color It is uniform. Using larger windows performance improves. One of the applications that would be interesting for thresholding pictures are very dark areas where objects are almost imperceptible to the human eye and yet no useful information in these regions. In local thresholding, the same object can be classified differently if your background is not constant, that is, if part of the is a dark area on either side of the on a clear area. This is a distinct disadvantage against global thresholding.

ISSN-On line: 2414-4924

Another drawback of the analyzed local thresholding is that they require a considerable number of parameters and that although the authors recommend parameters fixed, sometimes the best results using different parameters than those above. The fact that the images are taken for purposes of use in robotics and that the quality is not too high causes very noisy which can affect an algorithm with the characteristics of the local thresholding images. In terms of computational complexity of local thresholding require more operations, since each pixel performed in the case of Niblack 18 summations and 9 multiplications, in addition to the standard deviation calculation. In the case of Bernsen searches for minimum and maximum from 9 data. As for global thresholding only an amount per pixel for the histogram and a second sum and division to the cumulative histogram is performed. In the case of global thresholding, an image with a color irregular distribution could alter its functioning, so a good measure would apply a stretching algorithm in a pre-processing.

Referencias

[1] W. Niblack, An Introduction to Digital Image Processing. Prentice-Hall,
1986.

[2] J. Bersen, “Dynamic Thresholding of Grey-Level Images,” in Proc. of the 8th Int. Conf. on Pattern Recognition, 1986.

[3] http://www.cas.kth.se/IDOL/#Download.
[4] http://opencv.org/.

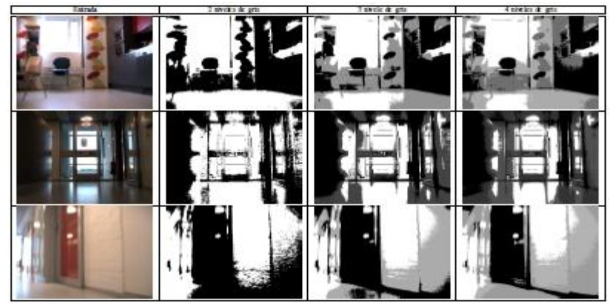

Table I Results from the global thresholding.

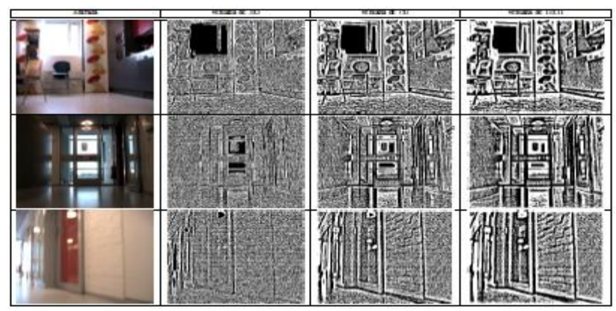

Table II Results obtained with thresholding algorithm Niblack.

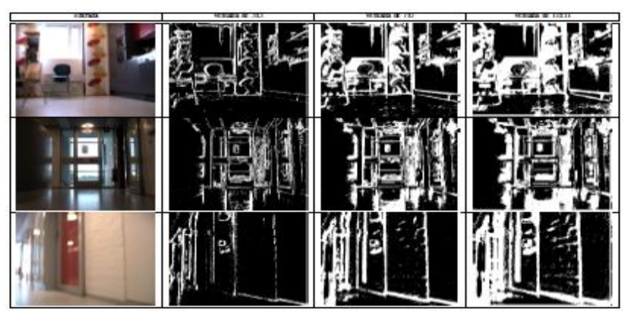

Table III Results obtained with thresholding algorithm Bernsen.

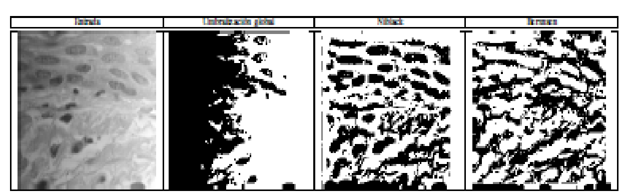

Table IV Comparison of the performance of different algorithms against the same image. In this case it is observed that the overall umbralizador not produce good results since the left side of the image is lightly shaded, which affects their performance. The algorithm with better results for this test is the Niblack.

Wavelets for correction of ECG images

AGUIRRE-RAMOS, H.*†

Universidad de Guanajuato. División de Ingenierías Campus Irapuato - Salamanca

Received July 31, 2015; Accepted October 30, 2015

Abstract

A method for removing noise in ECG signals consisting of the decomposition occurs at L level, the signal using a wavelet Daubechies. Each segment is analyzed to determine whether or not components are reduced or attenuated; modified from the original data signal is reconstructed preserving the values of CAL approximation and all those details CDi components whose contribution is relevant to the shape of the ECG signal. To determine if a signal should be preserved or not a rule based on the standard deviations of the reporting segment and the original signal is used.

ECG, noise, wavelet.

Citation: AGUIRRE-RAMOS, H. Wavelets for correction of ECG images. ECORFAN Journal-Democratic Republic of Congo 2015, 1-1: 36-41

* Correspondence to Author (email: wendy.cuevas@hotmail.com)
† Researcher contributing first author.

Introduction

The activity of the heart can be amplified and be recorded on an electrocardiogram *(ECG)*, which can be used to diagnose heart disease. With each heartbeat, an electrical signal spreads from the top to the bottom part thereof. This signal causes the walls of the heart to contract. When the walls contract, blood is pumped into the circulatory system. Internal and external to the chambers of the heart valves ensure that blood flow is in the right direction.

The typical layout of an electrocardiogram, as shown in Figure 1, consists of a P wave, a QRS complex and a T wave Small wave U is usually invisible. These are electrical events not to be confused with the corresponding mechanical events, ie the contraction and relaxation of the heart chambers. Thus, the mechanical systole or ventricular contraction begins just after the start of the QRS complex and ends just before the T wave end diastole is the relaxation and ventricular filling begins after culminating systole corresponding to the contraction of the atria, right after the start of the P wave This process is repeated for each heartbeat.

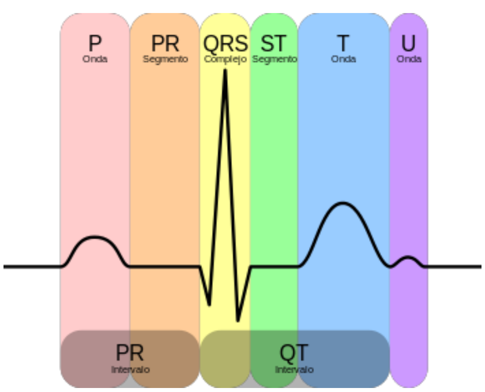

Figure 1 ECG Signal

The frequency of the ECG signal may be between 0.5 Hz and 100 Hz, this sen~ to be corrupted due to various types of devices, such as line interference power, noise contact with the electrodes, motion artifact, muscle contractions, baseline shift or noise generated by electronic equipment among others.

A corrupt signal these devices lead to misdiagnosis. Therefore, reduce and remove the noise contained in these signals is a starting point for the analysis thereof. In addition to conventional filtering techniques (FIR and IIR filters) [1], have been exploited other noise reducing means, such as using wavelets [2].

It is proposed to use the decomposition of the signal from the wavelet transform to suppress noise in the signal. This process is carried out by partial or total removal of detail coefficients that are generated from the decomposition of the signal.

Implementation

The overall process is illustrated in Figure 2, this process comprises the following steps:

- Signal reading and parameters
- Calculating reference values
- Signal decomposition
- Travel segments decomposition
  - Calculation of values of the segments
  - Reduction or elimination of components
- Signal Reconstruction

ISSN-On line: 2414-4924

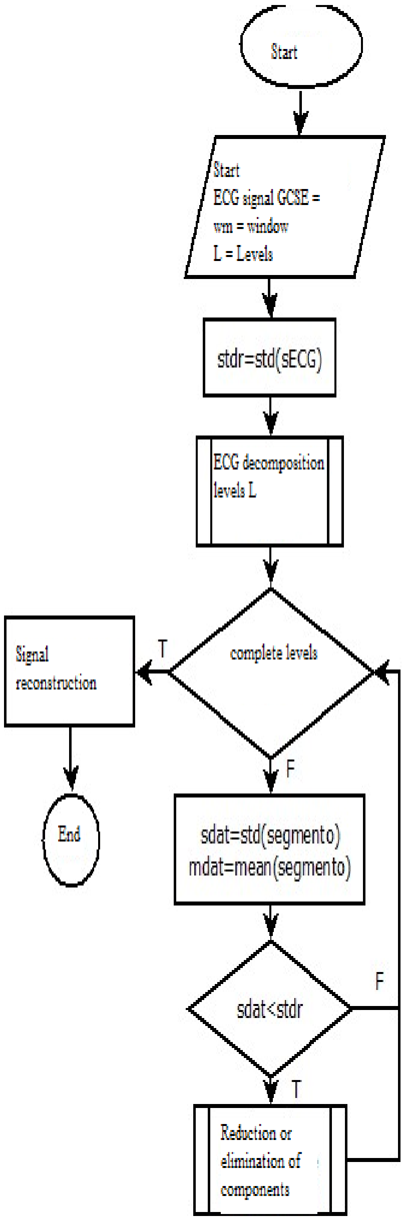

Figure 2 Overall process

A. Reading and signal parameters

Shown process is performed using MatLab programming environment; data from the study of electrocardiogram, stored in a CSV or XLS file is read and stored in memory for use for validating a synthetic ECG signal is generated from the individual functions $sECG=ecg(N)$ of MatLab.

The levels of decomposition and wavelet used are determined from experimentation with a synthetic signal and defined functions MatLab.

Decomposition of the signal B.

For the decomposition of the signal wavedec function of MatLab environment it is used. This function develops multi-level analysis to trave's of the application of a one-dimensional wavelet. It has the syntax: $[C,Le] = wavedec(X,N,'wname')$;

Returns the decomposition of N-level signal X using the mother wavelet *'wname'* in vector *C* and the length of each of these segments in the *Le* vector. Figure 3 shows the decomposition of S signal using 5 levels of decomposition.

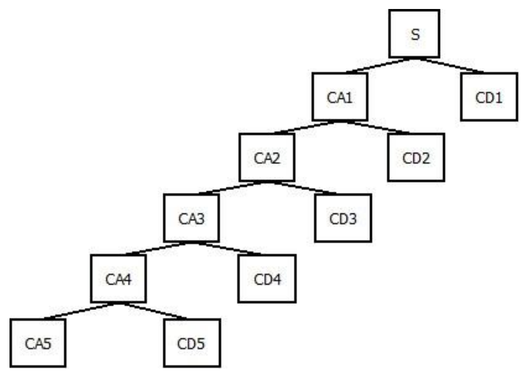

Figure 3 Breakdown of a signal into 5 levels

At each level of decomposition ISC CDi data and data is generated; the first coefficients corresponding to the approximation of the signal, while the latter contain coefficients details thereof. As the number of levels in the decomposition increases, coefficients generally ran CAI two new data sets and CA_{i+1} y CD_{i+1} $\forall i = 1,2,\ldots,L-1$. Consider the data shown in Table 1, these displayed ISC and CDi coefficients generated from the decomposition for L = 4, 5, 6 and 7 levels.

December 2015 Vol.1 No.1 36-41

C. Tour of the segments and elimination or reduction of components

Depending on the *L* value selected, the vector *C* will have *L +1* corresponding to the decomposition of the signal in the coefficients CA_L y $CD_i \quad \forall i = 1,2,\ldots,L$.

While the coefficients may be reduced or CDi entirely eliminated, the coefficients in CA_L

Levels	Data							
4	CA4				CD4	CD3	CD2	CD1
5	CA5			CD5	CD4	CD3	CD2	CD1
6	CA6		CD6	CD5	CD4	CD3	CD2	CD1
7	CA7	CD7	CD6	CD5	CD4	CD3	CD2	CD1

They are retained, then a route is through the CDi coefficients to determine whether they should be eliminated.

For each of the segments having the standard deviation is calculated, if the segment in question has a lower than that observed in the original signal standard deviation, this segment will be a candidate for the reduction of its components. Thus, segments with lower standard deviations correspond to elements listed throughout uniformly signal and therefore its contribution to the waveforms in the ECG will not be significant, corresponding mostly noise present in the signal.

Partial or total reduction will lead to a signal which retains most of its characteristics, not their amplitudes. Completely eliminate certain segments, for example, it produces a reduction in amplitude at the maximum or minimum *QRS* points of the signal to be treated. To prevent this effect, the following formula is used:

$$C_{seg}(n) = \begin{cases} 0 & |C_{seg}(n)| > \frac{\sigma_{seg}}{K} + \mu_{seg} \\ C_{seg}(n) & otherwise \end{cases} \qquad (1)$$

Where (n) is the value of the analyzed segment, while σseg and usec are the mean of this, with standard deviation and K≥4.

Consider the data in Table 2, with the contribution of each of the segments of a synthetic noise signal with uniform ADDED shown. Columns 3 and 4 show the average of each of the segments and standard deviation, which compared with the value of the standard deviation of the original signal (σ_{ref} = 0.2943) shows that the segments CD_1 to CD_4 are candidates reduction in its components. For these segments, the App column shows that these do not provide data to the waveform pseudo-noise but only along uniform signal.

Seg	App	σ_{seg}	μ
CD1	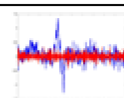	0.1879	-0.0017
CD2	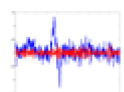	0.2124	0.0046
CD3	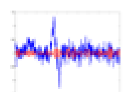	0.2306	-0.0258
CD4	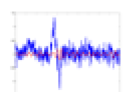	0.2121	-0.0047
CD5	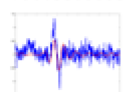	0.5837	0.0021
CD6	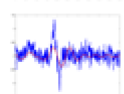	0.5614	-0.0158
CA6	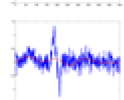	0.3886	0.5568

Table 2 Decomposition of an ECG signal with σ_{ref} = 0.2943 in 6 levels of wavelet decomposition using a DB34

Reconstruction of the signal D.

With the new vector C reduced, we proceed to the reconstruction signal for this function MatLab Wave-rec is used. This function takes C and Le vectors generated by the wavedec function, plus the type of wavelet decomposition used for reconstructing the original signal from these. It has the syntax:

ISSN-On line: 2414-4924

Article ECORFAN Journal
December 2015 Vol.1 No.1 36-41

Experimental results

There is a maximum level of decomposition that can be made to a signal; but generally 5, 6 or 7 levels can be performed without problem. Table 3 shows the correlation between a synthetic signal (without noise) and filtered versions of this (after the addition of noise). Data is filtered by using a threshold signal value K = 4, completely eliminating the corresponding segment and also applying the Savitzky-Golay filter MatLab, for 2-10 levels of decomposition. It is noted that the correspondence maximum levels are 4, 5, 6 and 7 levels of decomposition. Different tests showed a value of $L = 6$ generates good results, without increasing processing time.

Performing a similar process, but now alternating windows used, the most suitable for the task wavelet window was determined, showing that windows db28 DB34 and produce the best results in tests, the data are summarized in Table 4.

Using the information obtained noise reduction process of the synthetic signal is performed, producing the output shown in Figure 4. The data obtained through wavelet remain very close to those shown by the Savitzky-Golay filter in most 'ıa of its points.

$$else \qquad C_{seg}(n) = C_{seg}(n) \qquad (2)$$

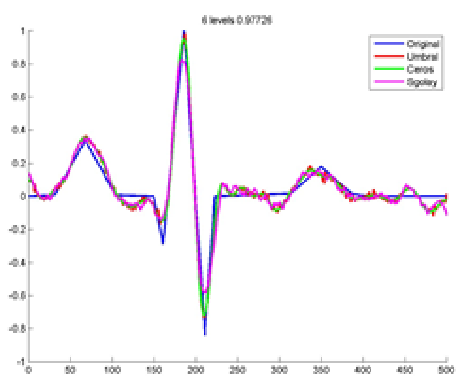

Figure 4 Filter a synthetic signal, using the process in Figure 2, with wn = DB34, L = 6 and K = 4.

Conclusions

Table 5 shows the relationship between the synthetic signal without noise and filtered versions of the same signal with white noise. Data show that noise reduction using wavelet following results using Savitzky-Golay; however it has a higher correlation with the original signal, which can be seen on the peaks of the QRS complex in Figure 4, where the Savitzky-Golay filter has a lower amplitude than the original signal using wavelet or results.

	Correlation(X_{fil} ,X_{or})
Thres	0.9761
Savitzky-Golay	0.9628

Table 5 Comparison of results

Following the same procedure the filtering process a sen~ the actual ECG is performed, resulting in the signal in Figure 5.

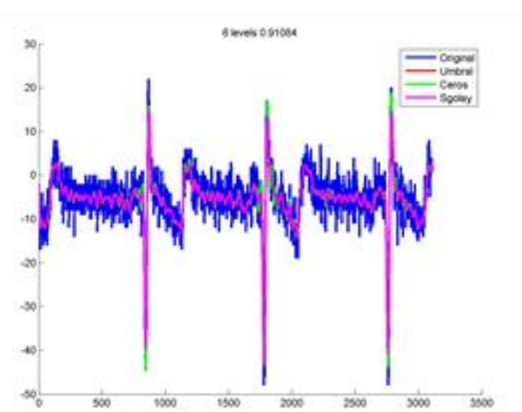

Figure 5 Noise reduction in real ECG signal with wn = DB34, L = 6 and K = 4

It is concluded that the use of wavelet on other filters produces similar or better outputs, reducing in most cases time for the filtration result.

ISSN-On line: 2414-4924

December 2015 Vol.1 No.1 36-41

Levels	2	3	4	5	6 7 8 9	10
Thres	0.9140	0.9639	0.9761	0.9761	0.9761 0.9648 0.9676	0.9642
Savitz ky-					0.9628	

Table 3 correlation with decomposition levels using a DB34 window.

Wavelet	db28	db34	dmey	bior2.2	bior6.8	rbio3.9	rbio6.8	coif4	sym16
Thres	0.9762	0.9761	0.9699	0.9588	0.9485	0.9640	0.9435	0.9727	0.9741
Savitzky-Golay					0.9628				

Table 4 Correlation of the filtered relative to the reference through several windows using 6 levels of decomposition signal.

References

[1] B. Chandrakar, O.P. Yadav, V.K. Chandra, “A survey of noisse removal techniques for ECG signals”, In- ternational Journal of Advanced Reserch in Compu- ter and Comnunicacion Engineering, vol. 2, no. 3, pp. 1354-1357, 2013

[2] S. Baduru, S. Reddy, P. Jagadamba, P. Satyanarayana, “Noise Cancellation on ECG and Heart Rate Signals Using the Undecimated Wavelet Transform”, Interna- tional Journal of Engineering Research and Applica- tions (IJERA), vol. 1, no. 4, pp. 1962-1970, 2011

Instructions for authors

A. Submission of papers to the areas of analysis and modeling problems of the:

- Image and Signal Processing
- Control
- Digital system
- Optimization
- Artificial Intelligence
- Fuzzy Logic
- Mathematical Modelling
- Computational Mathematics
- Computer Science

B. The edition of the paper should meet the following characteristics:

-Written in English. It is mandatory to submit the title and abstract as well as keywords. Indicating the institution of affiliation of each author, email and full postal address and identify the researcher and the first author is responsible for communication to the editor

-Print text in Times New Roman #12 (shares-Bold) and italic (subtitles-Bold) # 12 (text) and #9 (in quotes foot notes), justified in Word format. With margins 2 cm by 2 cm left-right and 2 cm by 2 cm Top-Bottom. With 2-column format.

-Use Calibre Math typography (in equations), with subsequent numbering and alignment right: Example;

$$\partial \rightarrow \frac{\partial y}{z} = \frac{1}{2} \tag{1}$$

-Start with an introduction that explains the issue and end with a concluding section.

- Items are reviewed by members of the Editorial Committee and two anonymous. The ruling is final in all cases. After notification of the acceptance or rejection of a job, final acceptance will be subject to compliance with changes in style, form and content that the publisher has informed the authors. The authors are responsible for the content of the work and the correct use of the references cited in them. The journal reserves the right to make editorial changes required to adapt the text to our editorial policy.

C. Items can be prepared by self or sponsored by educational institutions and business. The manuscript assessment process will comprise no more than twenty days from the date of receipt.

D. The identification of authorship should appear in a first page only removable in order to ensure that the selection process is anonymous.

E. Charts, graphs and figures support must meet the following:

-Should be self-explanatory (without resorting to text for understanding), not including abbreviations, clearly indicating the title and reference source with reference down with left alignment number 9 with bold typography.

-All materials will support gray scale and maximum size of 8 cm wide by 23 cm tall or less size, and contain all content editable.

- Graphic, Figures and Tables should be simple and present relevant information. Prototype;

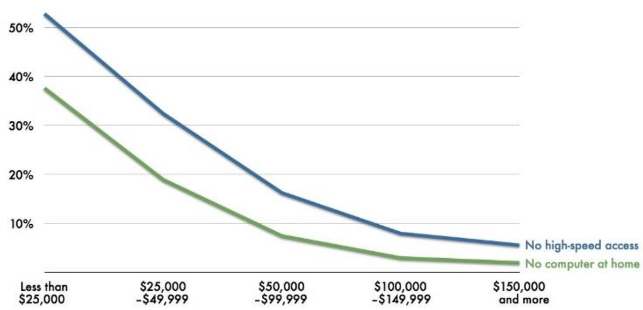

Graphic 1 Poor people have less access to high-speed internet and computers at home

F. References are included at the end of the document, all its components will be separated by a comma and must the following order:

- Articles: Nicholas, D., Watkinson, A., Jamali, H. R., Herman, E., Tenopir, C., Volentine, R., ... & Levine, K. (2015). Peer review: still king in the digital age. *Learned Publishing*, *28*(1), 15-21.

- Books: Schubert Jr, T. F., & Kim, E. M. (2015). *Fundamentals of Electronics: Book 2: Amplifiers: Analysis and Design*. Morgan & Claypool Publishers.

- WEB Resources: http://www.ebooks.com, see: (January, 16-2015)

The list of references should correspond to the citations in the document.

G. The notes to footnotes, which should be used and only to provide essential information.

H. Upon acceptance of the article in its final version, the magazine tests sent to the author for review. ECORFAN-Democratic Republic of Congo only accept the correction of types and errors or omissions from the process of editing the journal fully reserving copyright and dissemination of content. Not acceptable deletions, substitutions or additions which alter the formation of the article. The author will have a maximum of 10 calendar days for the review. Otherwise, it is considered that the author (s) is (are) in accordance with the changes made.

I.Append formats Originality and Authorization, identifying the article, author (s) and the signature, so it is understood that this article is not running for simultaneous publication in other journals or publishing organs.

Kinshasa, Democratic Republic of Congo ____, ____ 20_____

Originality Format

I understand and agree that the results are final dictamination so authors must sign before starting the peer review process to claim originality of the next work.

____

Article

____

Signature

____

Name

Kinshasa, Democratic Republic of Congo ____, ____ 20_____

Authorization Form

I understand and accept that the results of evaluation are inappealable. If my article is accepted for publication, I authorize ECORFAN to reproduce it in electronic data bases, reprints, anthologies or any other media in order to reach a wider audience.

____

Article

____

Signature

____

Name

ECORFAN Journal- Democratic Republic of Congo

“Brain Tumor and Vascular Structures Segmentation Applied in Computer Assisted Surgery”
ILUNGA-MBUYAMBA, Elisee and AVIÑA-CERVANTES, J. G.
Universidad de Guanajuato

“Kalman filter for skin-colored object tracking”
H.-AGUIRRE-RAMOS, J. G., AVINA-CERVANTES, E. and ILUNGA, Mbuyamba
Universidad de Guanajuato

“Bayesian classification of oranges using image processing”
ILUNGA-MBUYAMBA, Elisée and AVIÑA-CERVANTES, Juan GABRIEL
Universidad de Guanajuato

“Segmentation of vascular structures around brain tumors using region growing on Frangi vesselness”
ILUNGA-MBUYAMBA, Elisee, AVIÑA-CERVANTES, Juan Gabriel and AGUIRRE-RAMOS, Hugo
Universidad de Guanajuato

“Multiumbral optimal segmentation through a metaheuristic optimization algorithm”
MONTOYA-AGUILAR, Merary, CRUZ-DUARTE, Jorge Mario and AVIÑA-CERVANTES, Juan Gabriel
Instituto Tecnológico de Culiacán
Universidad de Guanajuato

“Thresholding images”
GARCÍA-MARTÍINEZ, Manuel Darío
niversidad de Guanajuato

“Wavelets for correction of ECG images”
AGUIRRE-RAMOS, H.
Universidad de Guanajuato

ISSN-On line: 2414-4924